공학 박사 학위 논문

A Study on the Pump Output Control of the Moving-Actuator Type Implantable Biventricular Assist Device

이동 작동기형 이식형 양심실 보조 장치의 펌프 박출량 제어에 관한 연구

2000 년 2 월

서울대학교 대학원
협동과정 의용생체공학 전공
엄 경 식

A Study on the Pump Output Control of the Moving-Actuator Type Implantable Biventricular Assist Device

이동 작동기형 이식형 양심실 보조 장치의
펌프 박출량 제어에 관한 연구

지도교수 민 병 구

이 논문을 공학박사 학위논문으로 제출함

1999년 10월

서울대학교 대학원
협동과정 의용생체공학 전공
엄 경 식

엄경식의 공학박사 학위논문을 인준함

1999년 12월

위 원 장 ______________________

부위원장 ______________________

위 원 ______________________

위 원 ______________________

위 원 ______________________

***Youth is the challenge against
the uncertain future.***

Abstract

The trend of artificial heart research has shifted to implantable system and the role of implantable ventricular assist device (VAD) has been amplified, for various reasons as time goes on. In this dissertation, the pump output (***PO***) control, for moving-actuator type implantable biventricular assist device (MA-BVAD), is discussed. There are three kinds of ***PO*** control methods for the VAD system: The fixed pump rate (***PR***), the fixed stroke volume (***SV***) (full-to-empty control), and the synchronous control. Various information of ***PO***, ***PR***, and so on must be externally monitored, whether the system is correctly operated or not.

In this research, a combined control architecture was adopted to effectively regulate the various types of controllers. For the biventricular assist controller, fixed ***SV*** controller, fixed ***PR*** controller, and heart rate (***HR***)-based controller were developed. As the preparation against heart attack, the total assist controller was developed. In particular, the fixed ***SV*** controller has been regarded as an important research, because of its reliable and reasonable ***PO***. For the ***SV*** controller, the parameter of end-diastole volume (EDV) is needed. Until now, interventricular pressure (***IVP***) has been utilized for MA-BVAD. ***IVP*** reflects the dynamic inflow state, but the pressure sensor is not robust enough against external disturbances. On the other hand, motor current is robust against external disturbances, but has not been properly considered because of its reflection of not only preload but also afterload for the active-filling devices.

In this research, a new preload-sensitive parameter, referred to as percent time before contact (***PTBC***) from motor current signal, was proposed for active filling-device such as our MA-BVAD. Since ***PTBC*** is good information for the EDV, this is used to construct the fixed ***SV*** and total assist controllers. *In vitro* and *in vivo* test showed that the developed fixed ***SV*** and total assist controllers perform well. The fixed ***PR*** controller was developed based on a simple rule-base. A new ***HR***-based controller was developed, by modifying synchronous controller for MA-BVAD, but this controller needs further verification through the *in vivo* test.

Finally, beat-to-beat mean ***PO*** and aortic pressure (***AoP***) estimators were developed, using ***PTBC*** and motor current. The developed ***PO*** estimator can cope with various situations of variable stroke angle, diastolic and systolic dynamics. The developed ***AoP*** estimator is derived from the energy equilibrium. The developed estimators have physical meaning, and *in vitro* test showed that they are reliable, even though their simplicity. For noise suppression in the motor current, a center weighted median (CWM) filter was studied. This filter enhances the precision of ***PTBC*** and the estimators. Experimental results showed that CWM filter with side-length two and central weight one is most appropriate in the perspectives of detail preservation and waveform.

Key word: Pump output, aortic pressure, artificial heart control, biventricular assist device

Student Number: 96431-803

Contents

List of Figures

List of Tables

Nomenclature

BVAD	:	Biventricular Assist Device
CWM	:	Center Weighted Median
ECG	:	Electrocardiography
EDV	:	End-Diastolic Volume
IND	:	Independent (mode)
LMA	:	Left Master Alternate (mode)
LMS	:	Least Mean Square
LUT	:	Look-Up Table
LVAD	:	Left Ventricular Assist Device
MA-BVAD	:	Moving-Actuator type Biventricular Assist Device
RMA	:	Right Master Alternate
ST	:	Sampling Time
TAH	:	Total Artificial Heart
TET	:	Transcutaneous Energy Transmission
VAD	:	Ventricular Assist Device
VVD	:	Variable Volume Device
WM	:	Weighted Median

AoP	:	Aortic Pressure
BT	:	Brake Time of the actuator (pause time at the left side) [msec]
BT_L	:	Left ***BT***
BT_R	:	Right ***BT***
CL	:	Current Level
CL_L	:	Left ***CL***

$\boldsymbol{CL_R}$	:	Right ***CL***
CO	:	Cardiac Output [*l*/min]
HR	:	Heart Rate [beats per minute]
IVP	:	Interventricular Pressure [mmHg]
LAP	:	Left Atrial Pressure
mAoP	:	Mean Aortic Pressure
mIVP	:	mean Interventricular Pressure [mmHg]
mLAP	:	Mean Left Atrial Pressure
mPAP	:	Mean Pulmonary Artery Pressure
mRAP	:	Mean Right Atrial Pressure
PAP	:	Pulmonary Artery Pressure
PDTR	:	Percent Diastolic Filling Time Ratio
PO	:	Pump Output [*l*/min]
PR	:	Pump Rate [beats per minute]
PTBC	:	Percent Time Before Contact
$\boldsymbol{PTBC_L}$	:	Left ***PTBC***
$\boldsymbol{PTBC_R}$	:	Right ***PTBC***
RAP	:	Right Atrial Pressure
SA	:	Stroke Angle [0.68 degree], (Hall sensor signal. As there are twenteen signals per one rotation of motor and the gear ratio is 44, 1 *SA* corresponds to 0.68 degree from 360°/12/44 [rad] = 0.68 °)
$\boldsymbol{SA_L}$	:	Left ***SA***
$\boldsymbol{SA_R}$	:	Right ***SA***
SV	:	Stroke volume
$\boldsymbol{SV_0}$	:	Geometric ***SV***, Full-fill/full-out ***SV***,
$\boldsymbol{SV_L}$	:	Left ***SV***

$\boldsymbol{SV_R}$	:	Right ***SV***
Vel	:	Velocity of the actuator [number of output of Hall sensor per second]
$\boldsymbol{Vel_L}$	:	Left ***Vel***
$\boldsymbol{Vel_R}$	:	Right ***Vel***

1. INTRODUCTION

1. 1. Background

Cardiovascular disease, the leading cause of death in developed countries, has also become the major cause of adult death in developing countries. The widespread use of long-term mechanical circulatory support systems can alleviate this problem and prolong life. Because of bioethical and social considerations, a genetically engineered method to replace or augment the failing heart's long-term function is not likely to be available commercially until after the year 2025 [1].

The mechanical circulatory support system can be categorized by: the total artificial heart (TAH), the biventricular assist device (BVAD), the left ventricular assist device (LVAD), and the right ventricular assist device (RVAD) in perspective of their roles. From a positional point of view, mechanical circulatory support systems are classified by: implantable, extracoporeal, and paracoporeal. For successful development of implantable artificial heart system, all related researches must be simultaneously considered and not one must be emphasized nor neglected. Even if it is debatable, we can categorize the research of implantable artificial heart system as in **Table 1. 1**.

The prospects of implantable VADs for clinical (therapeutic) use are hopeful. Implantable VADs have proved safe and beneficial for patients as a bridge to cardiac transplant. The ability of LVADs to support the circulation is undisputed. Chronic, sustained ventricular unloading is associated with improved native ventricular function. Reports show a reversal of maladaptive remodeling, an example being the reversal of chronic ventricular dilatation in patients with end-stage cardiomyopathy and the restoration of normal structure and biology. Another report indicates that mechanical support produced a reduction in anti-β_1 adrenoceptor autoantibodies and an improvement in cardiac function for nonishemic cardiomyopathy patients.

Table 1. 1. Implantable artificial heart research topic [2].

Division	Element	Consideration
1. Medicine	Surgical implantation	Blood and tissue-device duration
	Postoperative follow-up	Characterize device performance
	Exercise test	Describe organ function
	Autopsy and post explant device analysis	
2. Mechanics	Blood sac	Biocompatibility
	Actuator	Stability
	Motor	Reliability
	Chamber	Robustness
	Prosthetic valve	Safety
	Quick connector	Weight
	Cuff	Implantability
	Graft	Miniaturization
	Compliance system (window, chamber)	Controllability
	Oil	Flow characteristics
	Wire	Vibration
		Heat (temperature)
		Humidity
		Efficiency
		Lubrication
		Abrasion
		Sealing
		Aging effect
3. Materials	Blood contact materials	Hemocompatibility
	Cannula	Anticoagulation (thrombosis)
		Hemolysis
		Antibirus
4. Electronics	Implantable controller	*Stability*
and control	Transcutaneous energy transfer (TET) system	*Reliability*
	Internal and external battery	*Robustness*
	Telemetry	*Safety*
	Motor control	Heat (temperature)
	Hemodynamic estimation	Miniaturization
	Automatic control	*Efficiency*
	External monitoring	*Fault-tolerant*
	Remote monitoring	*Balanced output control*
	Alarm system	*Preload sensitive control*
	Sensor (Hall sensor, pressure, SvO_2)	*Afterload insensitive control*
		Controllability
		Observability
		Implementability
		Versatility
		Usability
		Position and velocity control
		PID motor control
		Sealing
		Aging effect
5. Etc	Application to VAD	
	Solar cell system	
	Acoustic signal processing	
	Simulation	

These findings suggest three therapeutic roles for VAD: 1) temporary support for “bridging” patients to a second procedure, 2) permanent support for end-stage heart failure, and 3) chronically unloading the heart, which promotes reversal of the maladaptive structural, hormonal, and biological processes that occur as heart failure progresses [56].

Whereas, the TAH research groups experienced many difficulties. One such problem is the TAH control system; this fact is aggravated by the removal of the native heart, thus eliminating the natural cardiac output (***CO***) control performed through the mechanoreceptors and chemoreceptors and also the left/right flow balance, which is helped by the native heart. This motivated the research of auxiliary TAH (ATAH) at Institute Dante Pazzanese of Cardiology and Baylor College of Medicine. This pump is characterized by a miniature size allowing implatation without removal of the native heart [34].

Since 1984, moving-actuator type total artificial heart (MA-TAH) has been developed at Seoul National University Hospital. At present, the applicability of MA-TAH to the moving-actuator type implantable biventricular assist device (MA-BVAD) has been studied. In this dissertation, *pump output* (***PO***) *control and the hemodynamic estimators for* MA-BVAD is studied. The implatable MA-BVAD has the following advantages in comparison to the TAH.

- Surgical risks are reduced from simple procedure, compared with a TAH implatation, for patients who still have some cardiac function.
- BVAD control is simpler than the TAH control, because of the requirement of only a small flow support function, rather than the total heart function.
- Left/right flow balance is not a critical factor for MA-BVAD control, because of the native heart’s function.
- Physiologic sensor information for MA-BVAD control, can be gathered by detection of native heart rate (***HR***).
- In the ultimate case of heart attack or breakdown of ***HR*** information, MA-BVAD can be

operated like the TAH.

- Better psychological effects on patient, because the weakened heart is not removed.

1. 2. Control of Native Heart and Artificial Heart

1. 2. 1. Control of the native heart

Figure 1. 1 shows the human circulatory system in simplified form [30]. The heart must adapt its performance to widely varying needs of the body, in order that each organ will receive enough blood to support its metabolic requirements. The limit of adaptation range from the minimum work needs during *sleep* to the maximum demands while performing *heavy exercise*. It is generally accepted that there are two mechanisms which occupies the activity of native heart. One is known as the *Frank-Starling mechanism* as an intrinsic regulation, and the other is the extrinsic regulation, i.e., the native heart is controlled by the *humoral and neural mechanisms* [31][28].

Pressure and flows in the *uncontrolled circulation* tend to be stabilized by the *Frank-Starling mechanism* which is plotted in **Figure 1. 2. (a).** The normal cardiovascular system has a more important stabilization mechanism as a result of *feedback control* acting through the *central nervous system*. This control depends on pressure signals that are converted to efferent nerve signals by the baroreceptors in the carotid arch. These nerve pathways are shown in **Figure 1. 2. (b)**. The heart can increase its work output by increasing the *rate* at which it contracts and by increasing the *force of contraction*, thereby ejecting more blood with each stroke. The force of contraction can be augmented by *humoral and neural mechanisms* which alter the metabolic state of the myocardium

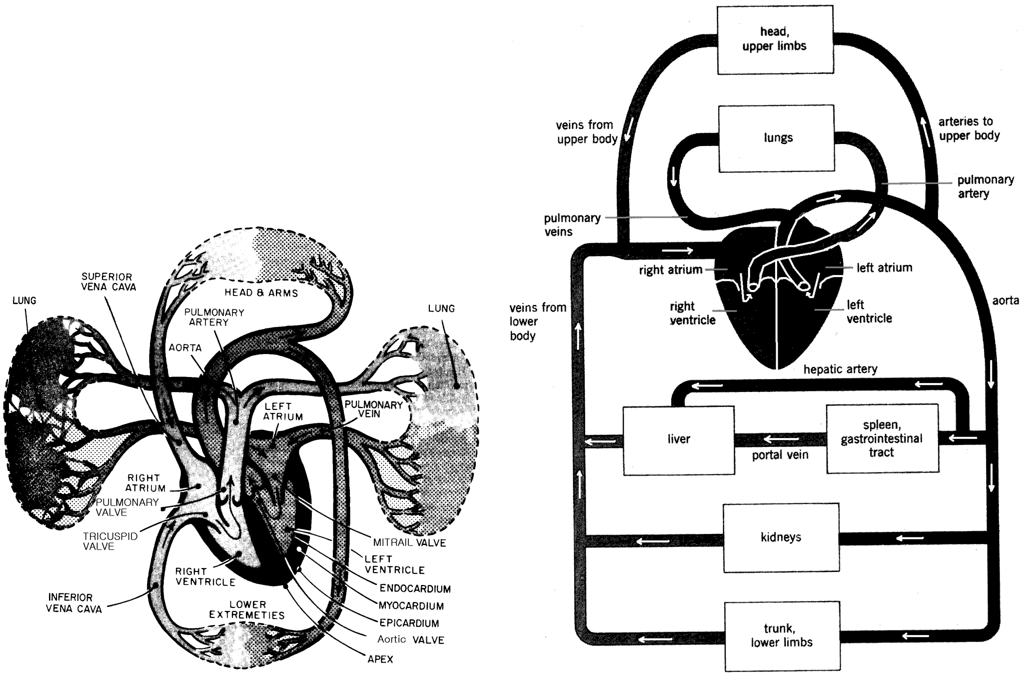

(a) (b)

Fig. 1. 1. The human blood circulatory system. (a) simplified form (Hewlet-Packard.), (b) block diagram form (Human Anatomy and Physiology, 2nd edition, by J. E. Crouch and R. McClintic, John Wiley & Sons, New York, 1976).

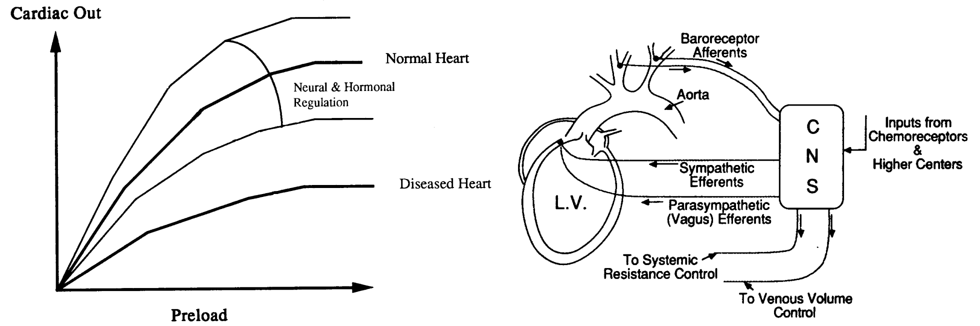

(a) (b)

Fig. 1. 2. (a) The rlationship between the preload and the cardiac output, (b) nerve pathways diagram [32].

or by *stretching the myocardium to increase its resting length or tension*. The *sympathetic fibers* have positive chronotropic (rate-increasing) and positive inotropic (force-increasing effects). The *parasympathetics* have a negative chronotropic effect and may be somewhat negatively inotropic, but the latter effect is, at most, small and is masked, in the intact circulatory system, by the increased filling which occurs when the diastolic filling time is increased [31].

1. 2. 2. Control of the ventricular assist device

The goal of the VAD *control* is as follow.

- ■ To reduce the ventricular pressure and volume work (ventricular decompression)

VAD system should have the capability for both *synchronous operation with the natural heartbeat* or *asynchronous operation*. Currently used control modes for VAD system are:

- ■ Fixed ***PR*** mode
- ■ Fixed ***SV***-variable rate (***VR***) mode (full-to-empty, pump-on-full, preload-sensitive)
- ■ Synchronous mode (Synchronized counterpulsation to the native heart)

Commercial or under development implantable VADs are shown in **Figure 1. 3.** Two implantable, vented VADs are in worldwide clinical use: HeartMate and Novacor. These systems are designed for a 2-year, high-reliability use. The US FDA has approved these devices as a bridge to cardiac transplantation. In Europe, these systems are additionally approved for long-term treatment of end-stage heart failure [56][57]. HeartMate has a precalibrated *stroke sensor* in the pump housing and this sensor can precisely measure and display the amount of blood at the end of the pump diastole and systole. The *asynchronous modes* include fixed-rate and pump-on-full (auto) options.

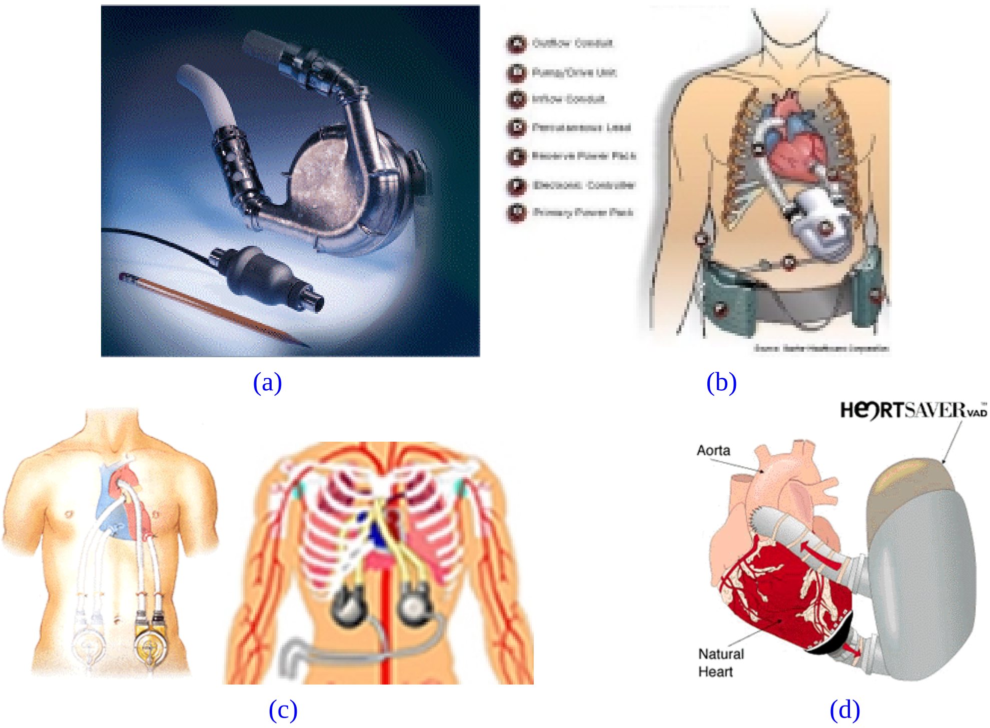

Fig. 1. 3. Implantable ventricular assist devices. (a) HeartMate (Thermo Cardiosystems Inc. (TCI), Woburn, MA), (b)Novacor (Novacor Division, Baxter Health Care Corp., Oakland, CA), (c) Thoratec (Thoratec Laboratories Co., Berkeley, CA), (d) Heartsaver (World Heart Corp.).

If set to operate in the auto mode, the device automatically ejects when the pump is 90% full (75 cc ***SV***). Conversely, with decreased filling, the LVAD slows to permit more time for filling. *Synchronization* of the pump is also possible with an *external QRS detector*. Clinical experience has shown that synchronization is not necessary and that the auto mode allows optimal decompression of the left ventricle and hemodynamics. The only other parameters that can be adjusted are eject duration and volume of the alarms. The Novacor LVAD has a nominal maximal ***SV*** of 70 cc, can provide ***PO*** in excess of 10 L/min, and can operate in *synchronous counterpulsation* at high cardiac rate (to 240 beats per minute). The longest supporting period (797 days) with the Novacor LVAD has been reported at Berlin German Heart Center in Germany, following which the patient was discharged [1].

1. 2. 3. Total assist control

In this dissertation, for the preparation of the heart attack, total assist control algorithm was developed. *The goal of the total assist control is same to the* TAH *control*.

- To mimic the native heart control

A tradeoff between *sensitivity* and *complexity* must be achieved to produce a TAH input control parameter that maintains metabolic homeostasis and an acceptable level of component reliability. The most important requirements of a TAH system are *to provide a physiologic flow rate while maintaining a safe* ***LAP***. The choice of control mode depends on the TAH *system used* and the *available control parameters*. *Full-to-empty* work without diaphragm standstill and *full stroke* is favorable with regard to anatomical fit and wash-out [33][12]. A control algorithm for a TAH should meet the following requirements [35].

- Simple and reliable
- Smallest physical package to meet anatomic constraints
- Adequate responses to all possible hemodynamic demands

There are two elements of Starlings work that are critical to TAH control theory:

- Afterload insensitivity: The vascular resistance to ejection must have a negligible effect on ***PO***.

■ Preload sensitivity: The volume of blood pumped by the heart is the rate of entry of blood in the heart primarily governed by end-disatolic volume (EDV).

Failure to match left/right ventricular flow with their respective vascular flow demands is termed *balance mismatching*, a situation causing venous congestion in the lagging circulation. It has been established that the net left ventricular ***PO*** exceeds the right ventricular ***PO*** by approximately 10% or more. It is generally agreed that *flow through the bronchial arteries* and *left sided valvular regurgitation* are the primary factors in this flow discrepancy between right and left ventricles [36].

■ Left and right balance: Enhancing left side flow efficiency by about 10% than right one with volume displacement system is the general target for alternate pumping.

Without humoral and neural mechanisms, tt is a lofty goal to attempt to achieve both left/right balance and variation in systemic flow in a total artificial heart through sensitivity to atrial pressure alone even if preload (atrium) sensitive and afterload (aorta) insensitive control is the popular artificial heart control [29].

From an engineering perspective, *alternate pumping* is preferable with regard to both design and size considerations. Left and right master alternate (LMA, RMA) control modes are version of *variable rate* control in which one pump serves as the master and the other as the slave.

■ Various studies showed that LMA mode control produces a higher performance than RMA one from various view points.

■ Animal studies have concluded that blood flow in the range of 80-140 ml/min/kg is necessary to maintain aerobic metabolism [36].

Although the ***PR*** can be increased to a higher range of 130-150 beat per minute [bpm], this may reduce the device durability. The physiological, pathological, and psychological consequences of using higher ***PR*** require further investigation [43]. Body acceleration has been shown to be sufficiently predictive of demand to be incorporated into commercial pacemakers and has been shown to correlate well with exercise intensity in calves [29][44].

1. 3. Objectives

The first objective of this research is *to develop the **PO** control algorithms and hemodynamic estimators for* MA-BVAD. The second one is *to verify their performance by in vitro and in vivo test.* The approach of this dissertation's research is characterized by the usage of the motor current signal. And, the following studies were carried out to accomplish the overall objectives.

- Proposal of 'percent time before contact (***PTBC***)' as a new preload-sensitive parameter for MA-BVAD
- Study of the center weighted median (CWM) filter, for the suppression of undesirable noise in motor current signal
- Development of control algorithms for MA-BVAD: fixed ***PR*** control, fixed ***SV*** control, and ***HR***-based control
- Development of beat-to-beat mean ***PO*** and aortic pressure (***AoP***) estimators
- Development of a total assist control algorithm as the preparation against heart attack

2. MATERIALS AND METHODS

The block diagram of this research is shown in **Figure 2. 1**. In this dissertation, motor current was selected to find the hemodynamic parameters. For noise suppression, the motor current signal is preprocessed by CWM filter. With the filtered motor current, ***PTBC*** as a preload-sensitive parameter, beat-to-beat mean ***AoP*** estimator, and beat-to-beat mean ***PO*** estimator were constructed. For the biventricular assist control, three kinds of control modes was studied: the fixed ***PR*** control, the fixed ***SV*** control, and the ***HR***-based control. The limiter inhibits the undesirable high deviation of the biventricular assist control output. When heart attack occurs, the biventricular assist control mode must be switched to the total assist control mode.

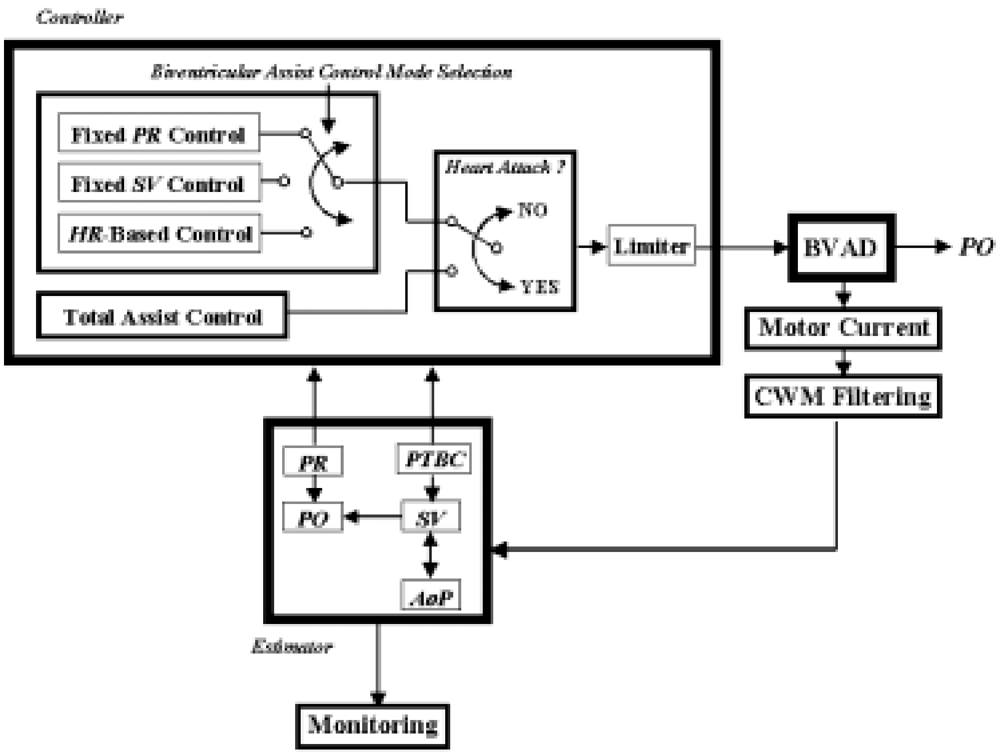

Fig. 2. 1. Block diagram of the objectives of this research.

2. 1. System Description of the Moving-Actuator Type Implantable Biventricular Assist Device

The MA-BVAD system consists of three major components: the moving actuator, the left ventricle, and the right ventricle. The actuator uses a brushless DC motor (S/M 566-20; Sierracin / Magnedyne, Carlsbad, CA, USA), which is moved in a pendular motion by an epicyclic gear train. Each ventricle is composed of polyurethane (Pellethane ®, Dow Chemical, Midland, MI, USA) double sacs. The pump height is 110 mm, width is 88 mm, thickness is 66 mm. The pump system weighs about 750 g. The left and right blood sac volumes are changed from (241 cc, 101 cc) to (102 cc, 91 cc) and currently changed to (84 cc, 71 cc). A rigid housing (Isoplast 301) contains the actuator and two ventricles. For the purpose of lubrication and heat dissipation, approximately 30% of the space between the actuator and the blood sacs is filled with silicon oil (FS-1265, 70 cc, Dow Corning USA), and the remaining 70 % with air. The air trapped insided the rigid pump housing is compressed or expanded to accommodate this interventricular volume change. The compliance window is made of polyurethane (Pellethane ® 2363-80AE: Dow Chemical USA). The area of compliance window is 56 $\times$90 mm. The compliance window together with the inside air plays the role of minor passive filling, the prevention of high negative pressure, and the balanced output. This pendular moving actuator device has advantages due to its unique configuration. First, it saves the dead space that would be occupied by the motor in a fixed actuator and it provides closer inflow and outflow port configuration than would be the case in a linear motion actuator. Second, it has a time-varying contact area between the actuator and each ventricle, providing different stroke volume trajectory between the two ventricles during the period of one stroke [3][4]. A schematic diagram and external view together with the implantable controller of our MA-BVAD is shown in **Figure 2. 2**. The pressure sensor for the measuring of interventricular pressure (***IVP***) is attached (NPI-19A-015GV, NOVA, USA). The interventricular space's volume is changed dynamically by the difference between the ejected volume of the systolic phase and the inflowed volume of the diastolic phase. The port connector is made of acetals. In the inflow and outflow ports, 29 mm and 25 mm valves (Bjork-Shiley mechanical tilting disc valve, Medtronics Hall valve, floating and flapping polyurethane valve) were used.

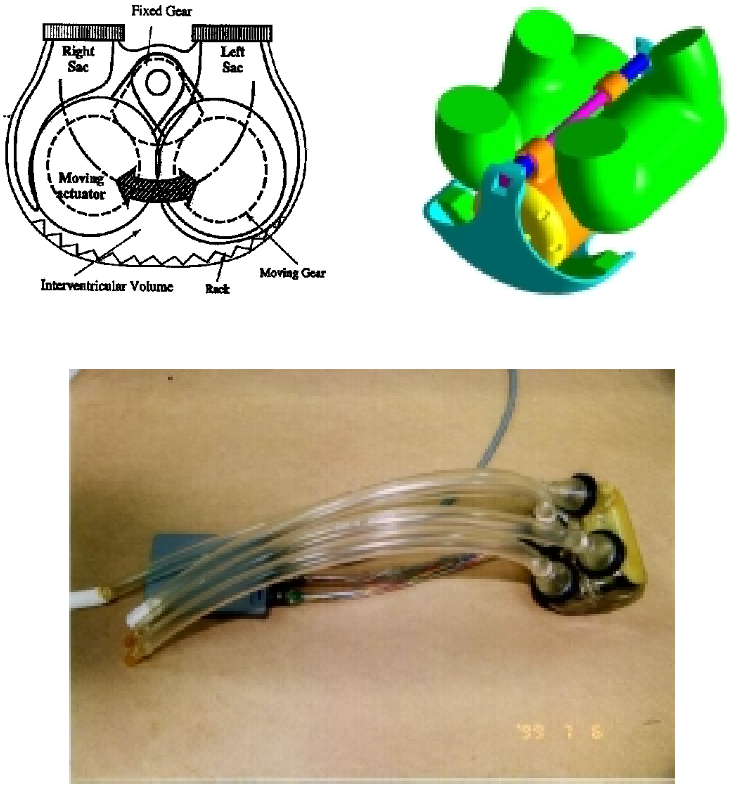

Fig. 2. 2. Moving-actuator type implantable BVAD.

2. 2. Modeling of Pump Output (*PO*)

The modeling techniques can be categorized by **Table 2. 1**. The detailed techniques can be divided into two classes. One is the approach of mathematical model [5][6][7], and the other is the input/output data-based approach [8][9][10]. Here, 'static state model' means that it does not use the previous state, contrarily, the 'dynamic state one' uses the previous state. The electric circuit model is one of dynamic models, as it requires the previous state depending on a time variable. Not only the control point of view, but also other ones such as display, database for management, and practical implementation (microcontroller, e.g., 80C196), the mean values of hemodynamics rather than dynamic ones are more favorite.

Mathematical model has merits of physical meaning and easiness of handling of model's constants. If there are changes in the constants in the system, we need not set up the model again but need change only the corresponding constants. Even if a mathematical model is set up, constant tuning with real situations or data must be followed. For this purpose, various methods are known such as pseudoinverse, LMS algorithm, recursive least square (RLS) algorithm, Kalman filtering algorithm, genetic algorithm [11], fuzzy logic, artificial neural network, etc.

In this dissertation, the mathematical model-based static state ***PO*** and ***AoP*** estimators are presented. And the proposed model consists of a combination of some parameters multiplied by corresponding constants. Proposed models can use *pseudoinverse* or *least mean square* (LMS) algorithm to match the real data to adjust model's constants.

CO is the multiplication of the ***SV*** by the ***HR***.

$$CO = SV \times HR \tag{2-1}$$

Likewise, the ***PO*** is the multiplication of ***SV*** by ***PR***.

$$PO = SV \times PR \tag{2-2}$$

Table 2. 1. Categorization of modeling technique. If the model does or does not use previous state, it is called a dynamic or static state model, respectively.

	Dynamic state model	Static state model
Mathematical model -based approach	Electric circuit model	*Developed PO estimation* *Developed AoP estimation*
Input/output data -based approach	Kalman filtering model Fuzzy Logic model Artificial neural network model	Multidimensional Interpolation Fuzzy Logic model Artificial neural network model

As ***PR*** is the given information, the problem of ***PO*** estimation is simply shifted to the ***SV*** estimation. Proposed approach for the ***SV*** estimation is to divide the ***SV*** function into three kinds of functions like

$$\begin{aligned} SV &= f_0(SA_L, SA_R) \times f_d(\textit{filling state}) \times f_s(mAoP) \\ &= SV_0 \times f_d(\textit{filling state}) \times f_s(mAoP) \end{aligned} \tag{2-3}$$

where SA_L and SA_R represent the left stroke angle and the right stroke angle, respectively. And, SV_0 represents the maximal possible stroke volume in the sense of the designed volume (full-fill/full-out ***SV***, geometric ***SV***). If the target ***PO*** is a right-sided flow, there is only required the replacement of f_s (***mAoP***) to f_s (***mPAP***). After SV_0 is calculated, two other points must be considered. One is the case of a not complete filling (f_d (***filling state***): *diastolic dynamics*) and the other is the case of regurgitation flow (f_s (***mAoP***): *systolic dynamics*). The blood sac is not completely inflated, and the regurgitation flow is dependent on ***mAoP***. Considering these points, required conditions are summarized as follows.

- ***SV condition 1***: $SV \le SV_0$
- ***SV condition 2***: $0 \le f_d$ (***filling state*** $\neq$100 %) < 1
- ***SV condition 3***: f_d (***filling state*** = 0 %) = 0

■ ***SV condition 4***: f_d (***filling state*** = 100 %) = 1

■ ***SV condition 5***: 0 < f_s (***mAoP*** ≠ 0) < 1

There are various factors which contribute to the regurgitation flow, but the major factor is known as the valvular regurgitation for electromechanical pumping system. It is commonly agreed that the forward flow decreases by about 10 % with load of about 100 mmHg and the slope is about –10 % with load of 100 mmHg for mechanical valve [12][13][14]. At first, the case of regurgitation flow can be considered like f_s (***mAoP***) = 1- c_2***mAoP***. For mechanical valve, f_s (***mAoP*** = 100 [mmHg]) = 0.9 = 1 - 100c_2, and c_2 = 0.001. Namely, c_2 is the characteristic constant (regurgitation flow) dependent on the valve type. Polymer valves are known to have smaller c_2 than mechanical valves. Of course, more complex function of f_s (***mAoP***) can be thought, but the tradeoff between the precision and complexity must be considered.

$$f_s(\boldsymbol{mAoP}) = 1 - c_2\boldsymbol{mAoP} \qquad (2\text{-}4)$$

The method to remove the impulsive noise terms in the motor current signal is stated in **Section 2. 2. 1**. The method to find SV_0, f_d (***filling state***) , and ***mAoP*** are studied exhaustively in **Section 2. 2. 2**, **2. 2. 3,** and **2. 2. 4**, respectively.

2. 2. 1. Center weighted median (CWM) filter

The removal of impulsive noise terms, which occur in motor current signal of an MA-BVAD, is necessary before ***PO*** estimation and ***PTBC*** calculation (see **Figure. 2. 3**). Mean-class linear filters not only have lower performance of removing impulsive noise, but also cause the distortion of the waveform. Nonlinear signal processing is essential for nonlinear signal problems. Impulsive noise, like the one that occurs in motor current, is a typical example. Especially, when the telemetry system is incorporated, the transmission error produces not Gaussian-like, but impulsive-like noise. To cope with this problem, CWM filter is considered in this study.

Nonlinear signal processing has led to the identification of four major, partially overlapping, families of nonlinear techniques: Order statistics (OS) based techniques, polynomial based algorithms, morphological methods, and homomorphic systems [21][22]. The selected approach is OS based filters. It is well known that CWM filter is an useful detail-preserving smoother and outperforms the median filter [23]. The CWM filter has a higher ability to conserve detailed signal components while removing impulse type noise than median filter. And, CWM filter has a simple structure and a low cost of operation.

CWM filter is a special case of the weighted median (WM) class filter. The weighted median (WM) filter generates $\boldsymbol{h}(\boldsymbol{j})$ copies of $\boldsymbol{X}(\boldsymbol{i}\text{-}\boldsymbol{j})$ for each $\boldsymbol{j} \in \boldsymbol{W}$. Then the output of a WM filter $\boldsymbol{Y}(\boldsymbol{i})$ is represented as

$$\boldsymbol{Y}(\boldsymbol{i}) = \boldsymbol{median}\{\boldsymbol{h}(\boldsymbol{j})\ \boldsymbol{copies\ of}\ \ \boldsymbol{X}(\boldsymbol{i}-\boldsymbol{j}) \mid \boldsymbol{j} \in \boldsymbol{W}\}. \tag{2-5}$$

The WM filter with central weight $\boldsymbol{h}(0) = 2\boldsymbol{w}+1$ and $\boldsymbol{h}(\boldsymbol{j}) = 1$ for each $\boldsymbol{j} \neq 0$ is called CWM filter, where $\boldsymbol{w}$ is a non-negative integer [23]. The output $\boldsymbol{Y}(\boldsymbol{i})$ of the CWM filter is given by

$$\boldsymbol{Y}(\boldsymbol{i}) = \boldsymbol{median}\{\boldsymbol{X}(\boldsymbol{i}-\boldsymbol{j}),\ 2\boldsymbol{w}\ \boldsymbol{copies\ of}\ \ \boldsymbol{X}(\boldsymbol{i}) \mid \boldsymbol{j} \in \boldsymbol{W}\}. \tag{2-6}$$

When $\boldsymbol{w} = 0$, the CWM filter becomes the median filter, so the median filter is a special case of a CWM filter. When $2\boldsymbol{w}+1$ is greater than or equal to the window size $2\boldsymbol{L}+1$, it becomes the identity filter (no filtering). Conversely, a CWM filter with a larger central weight performs better in detail preservation but worse in noise suppression than one with a smaller central weight.

For CWM and median filters, among various operation, comparison has higher load than other ones, so fast running ordering algorithms [24][25][26][27] or simplified algorithm like $\boldsymbol{Y}(\boldsymbol{i}) = \boldsymbol{median}\ \{\boldsymbol{X}(\boldsymbol{L}+1\text{-}\boldsymbol{w};\ 2\boldsymbol{L}+1),\ \boldsymbol{X}(\boldsymbol{L}+1+\boldsymbol{w};\ 2\boldsymbol{L}+1),\ \boldsymbol{X}(\boldsymbol{i})\}$ can be considered (see, **Appendix**).

2. 2. 2. Geometric stroke volume (SV_0)

In this section, cylindrical model, i.e., moving-actuator and blood sacs are assumed cylinders, is introduced to model $\boldsymbol{SV_0}$ which is a function of left and right stroke angle ($\boldsymbol{SA_L}$, $\boldsymbol{SA_R}$) [15]. The $\boldsymbol{SV_0}$ is the crossed area between two circles. Let's consider the simple case of **Figure 2. 3 (a)**. In this figure,

$$\theta_1 = \cos^{-1}\left(\frac{\boldsymbol{R}_1^2 + \boldsymbol{d}^2 - \boldsymbol{R}_2^2}{2\boldsymbol{R}_1\boldsymbol{d}}\right) \tag{2-7}$$

and

$$\theta_2 = \cos^{-1}\left(\frac{\boldsymbol{R}_2^2 + \boldsymbol{d}^2 - \boldsymbol{R}_1^2}{2\boldsymbol{R}_2\boldsymbol{d}}\right) \tag{2-8}$$

where

$$\boldsymbol{d} = \sqrt{\boldsymbol{L}_1^2 + \boldsymbol{L}_2^2 - 2\boldsymbol{L}_1\boldsymbol{L}_2\cos\theta} \tag{2-9}$$

Then

$$\begin{aligned} \boldsymbol{S}_1 &= \frac{1}{2}\boldsymbol{R}_1^2(2\theta_1) - \frac{1}{2}\boldsymbol{R}_1\cos(\theta_1)\boldsymbol{R}_1\sin(\theta_1)2 \\ &= \frac{1}{2}\boldsymbol{R}_1^2(2\theta_1 - \sin(2\theta_1)) \end{aligned} \tag{2-10}$$

and

$$\boldsymbol{S}_2 = \frac{1}{2}\boldsymbol{R}_2^2(2\theta_2 - \sin(2\theta_2)) \tag{2-11}$$

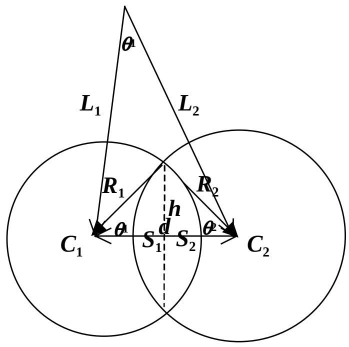

(a)

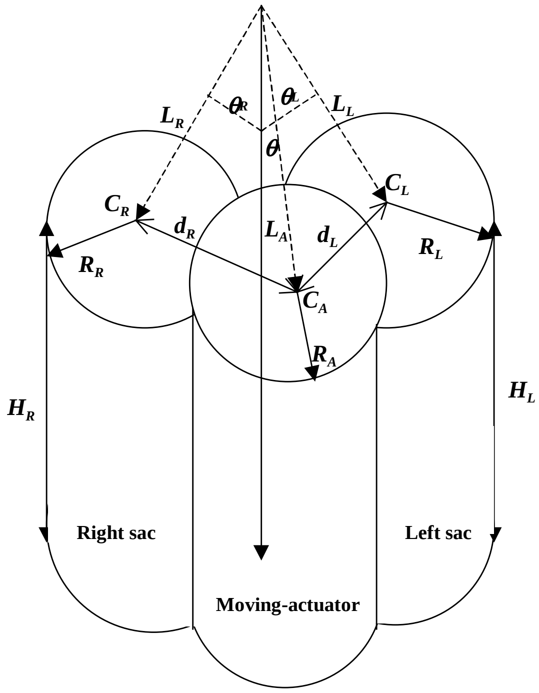

(b)

Fig. 2. 3. Cylindrical model for the MA-BVAD.

The cross area ***S*** between two circles is

$$\begin{aligned} \boldsymbol{S} &= \boldsymbol{S}_1 + \boldsymbol{S}_2 \\ &= \frac{1}{2}\boldsymbol{R}_1^2(2\theta_1 - \sin(2\theta_1)) + \frac{1}{2}\boldsymbol{R}_2^2(2\theta_2 - \sin(2\theta_2)) \end{aligned} \tag{2-12}$$

From this results we can set up $\boldsymbol{SV_L}$ like (See **Figure 2. 3. (b)**)

$$\begin{aligned} \boldsymbol{SV_L} &= \boldsymbol{S}_{L1}\boldsymbol{H}_L - \boldsymbol{S}_{L2}\boldsymbol{H}_L \\ &= (\boldsymbol{S}_{L1} - \boldsymbol{S}_{L2})\boldsymbol{H}_L \end{aligned} \tag{2-13}$$

where

$$\boldsymbol{S}_{L1} = \frac{1}{2}\boldsymbol{R}_A^2(2\theta_{AL1} - \sin(2\theta_{AL1})) + \frac{1}{2}\boldsymbol{R}_L^2(2\theta_{LA1} - \sin(2\theta_{LA1})) \tag{2-14}$$

$$\theta_{AL1} = \cos^{-1}\left(\frac{\boldsymbol{R}_A^2 + \boldsymbol{d}_{L1}^2 - \boldsymbol{R}_L^2}{2\boldsymbol{R}_A\boldsymbol{d}_{L1}}\right) \tag{2-15}$$

$$\theta_{LA1} = \cos^{-1}\left(\frac{\boldsymbol{R}_L^2 + \boldsymbol{d}_{L1}^2 - \boldsymbol{R}_A^2}{2\boldsymbol{R}_L\boldsymbol{d}_{L1}}\right) \tag{2-16}$$

$$\boldsymbol{d}_{L1} = \sqrt{\boldsymbol{L}_A^2 + \boldsymbol{L}_L^2 - 2\boldsymbol{L}_A\boldsymbol{L}_L\cos(\theta_{L\max} - \theta_L)} \tag{2-17}$$

$$\boldsymbol{S}_{L2} = \frac{1}{2}\boldsymbol{R}_A^2(2\theta_{AL2} - \sin(2\theta_{AL2})) + \frac{1}{2}\boldsymbol{R}_L^2(2\theta_{LA2} - \sin(2\theta_{LA2})) \tag{2-18}$$

$$\theta_{AL2} = \cos^{-1}\left(\frac{\boldsymbol{R}_A^2 + \boldsymbol{d}_{L2}^2 - \boldsymbol{R}_L^2}{2\boldsymbol{R}_A\boldsymbol{d}_{L2}}\right) \tag{2-19}$$

$$\theta_{LA2} = \cos^{-1}\left(\frac{\boldsymbol{R}_L^2 + \boldsymbol{d}_{L2}^2 - \boldsymbol{R}_A^2}{2\boldsymbol{R}_L\boldsymbol{d}_{L2}}\right) \tag{2-20}$$

$$\boldsymbol{d}_{L2} = \sqrt{\boldsymbol{L}_A^2 + \boldsymbol{L}_L^2 - 2\boldsymbol{L}_A\boldsymbol{L}_L\cos(\theta_{L\max} + \theta_R)} \tag{2-21}$$

Symmetrically, the $\boldsymbol{SV_R}$ is

$$\begin{aligned}\boldsymbol{SV_R} &= \boldsymbol{S_{R1}H_R} - \boldsymbol{S_{R2}H_R} \\ &= (\boldsymbol{S_{R1}} - \boldsymbol{S_{R2}})\boldsymbol{H_R}\end{aligned} \tag{2-22}$$

where

$$\boldsymbol{S_{R1}} = \frac{1}{2}\boldsymbol{R_A^2}(2\theta_{\boldsymbol{AR}1} - \sin(2\theta_{\boldsymbol{AR}1})) + \frac{1}{2}\boldsymbol{R_R^2}(2\theta_{\boldsymbol{RA}1} - \sin(2\theta_{\boldsymbol{RA}1})) \tag{2-23}$$

$$\theta_{\boldsymbol{AR}1} = \cos^{-1}\left(\frac{\boldsymbol{R_A^2} + \boldsymbol{d_{R1}^2} - \boldsymbol{R_R^2}}{2\boldsymbol{R_A d_{R1}}}\right) \tag{2-24}$$

$$\theta_{\boldsymbol{RA}1} = \cos^{-1}\left(\frac{\boldsymbol{R_R^2} + \boldsymbol{d_{R1}^2} - \boldsymbol{R_A^2}}{2\boldsymbol{R_R d_{R1}}}\right) \tag{2-25}$$

$$\boldsymbol{d_{R1}} = \sqrt{\boldsymbol{L_A^2} + \boldsymbol{L_R^2} - 2\boldsymbol{L_A L_R}\cos(\theta_{\boldsymbol{R}\max} - \theta_{\boldsymbol{R}})} \tag{2-26}$$

$$\boldsymbol{S_{R2}} = \frac{1}{2}\boldsymbol{R_A^2}(2\theta_{\boldsymbol{AR}2} - \sin(2\theta_{\boldsymbol{AR}2})) + \frac{1}{2}\boldsymbol{R_R^2}(2\theta_{\boldsymbol{RA}2} - \sin(2\theta_{\boldsymbol{RA}2})) \tag{2-27}$$

$$\theta_{\boldsymbol{AR}2} = \cos^{-1}\left(\frac{\boldsymbol{R_A^2} + \boldsymbol{d_{R2}^2} - \boldsymbol{R_R^2}}{2\boldsymbol{R_A d_{R2}}}\right) \tag{2-28}$$

$$\theta_{\boldsymbol{RA}2} = \cos^{-1}\left(\frac{\boldsymbol{R_R^2} + \boldsymbol{d_{R2}^2} - \boldsymbol{R_A^2}}{2\boldsymbol{R_R d_{R2}}}\right) \tag{2-29}$$

$$\boldsymbol{d_{R2}} = \sqrt{\boldsymbol{L_A^2} + \boldsymbol{L_R^2} - 2\boldsymbol{L_A L_R}\cos(\theta_{\boldsymbol{R}\max} + \theta_{\boldsymbol{L}})} \tag{2-30}$$

The simulated result of the derived $\boldsymbol{SV_0}$ is shown in **Figure 2. 4**. And, **Table 2. 2** is the data used which was acquired from the mechanical drawing. The results were simulated by Matlab 6.0. **Figure**

2. 4 and **2. 5** show that the ***SV*** between the actuator and blood sac increases exponentially with the increase of stroke angle (***SA***).

Table 2. 2. Constants for the geometric $\boldsymbol{SV_0}$ model.

Constants	Value
$\boldsymbol{L_a}$	2.6 cm
$\boldsymbol{L_L}$	2.6 cm
$\boldsymbol{L_R}$	2.6 cm
$\boldsymbol{R_A}$	2.0 cm
$\boldsymbol{R_L}$	2.1 cm
$\boldsymbol{R_R}$	2.0 cm
$\boldsymbol{H_L}$	8.7 cm
$\boldsymbol{H_R}$	8.0 cm
θ_L	$\pi/4$ rad
θ_R	$\pi/4$ rad
Left ventricular volume	8.7 * phi * 2.1*2.1 = 120 cc
Right ventricular volume	8.0 * phi * 2.0*2.0 = 100 cc

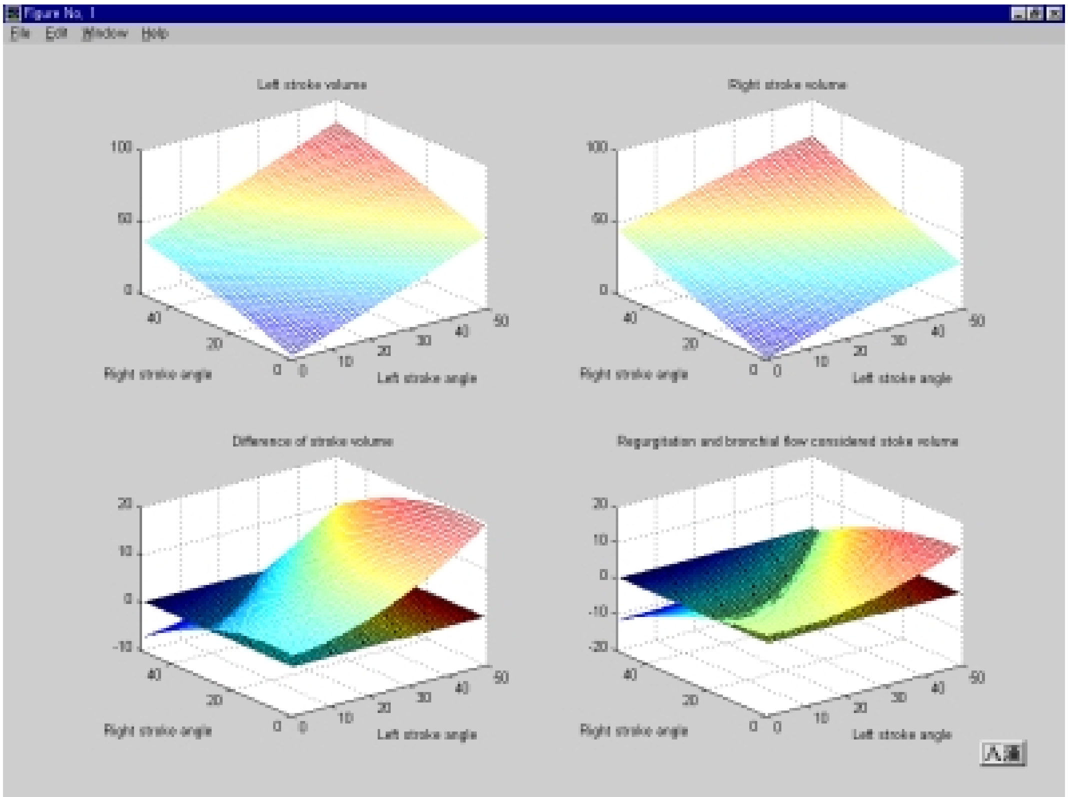

(a)

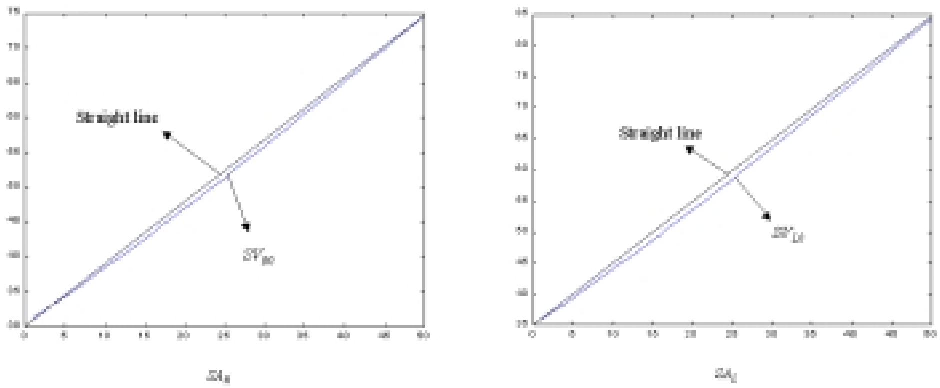

(b) (c)

Fig. 2. 4. ***SV_0***. (a) three dimensional plot, (b) ***SV_{R0}***, ***SA_L*** = 50, (c) ***SV_{L0}***, ***SA_R*** = 50.

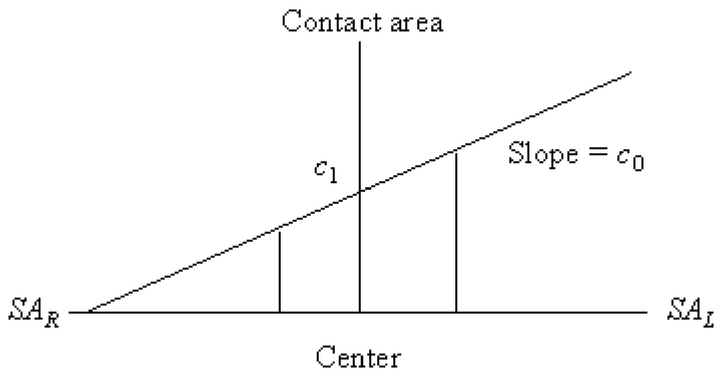

Fig. 2. 5. The relationship between ***SA*** and the contact area.

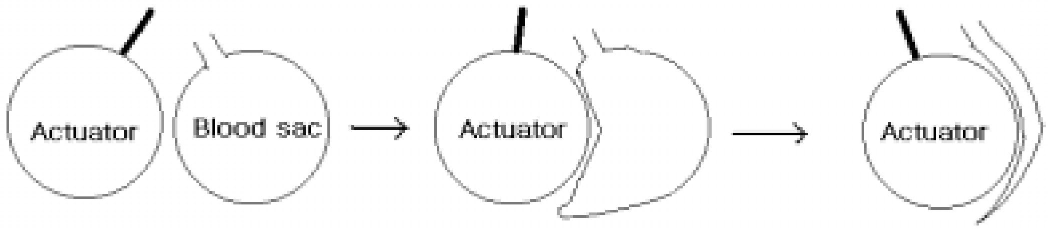

Fig. 2. 6. Shape of the flexible blood sac during ejection phase.

As the Eq. (2-13) requires high operational burden such as root, $\cos^{-1}\theta$, and $\sin\theta$. Moreover, during ejection the flexible blood sac is reshaped and the blood is displaced radially, so the previous model does not have a deep relation with a practical system. **Figure. 2. 6** shows the real shape of blood sac during systolic period. If we assume the contact area between the actuator and the blood sac increases with the increase of the ***SA***, we can simplify left $\boldsymbol{SV}_0$ like:

$$\begin{aligned} \boldsymbol{SV}_{L0} &= \int_0^{SA} (\textbf{contact area})\,\boldsymbol{dx} \\ &= \int_0^{SA_L} (c_0 x + c_1)\,\boldsymbol{dx} + \int_0^{SA_R} (-c_0 x + c_1)\,\boldsymbol{dx} \\ &= \frac{1}{2} c_0 \left(SA_L^2 - SA_R^2\right) + c_1\left(SA_L + SA_R\right) \\ &\sim c_0 \left(SA_L^2 - SA_R^2\right) + c_1\left(SA_L + SA_R\right) \end{aligned} \tag{2-31}$$

This equation shows that $\boldsymbol{SA_L}$ has a higher contribution to the $\boldsymbol{SV_{L0}}$ than $\boldsymbol{SA_R}$.

2. 2. 3. *PTBC* as a preload-sensitive parameter

A preload-sensitive parameter is required to construct the presload-sensitive control of MA-BVAD and to find the $\boldsymbol{f_d}$ (***filling state***) for ***PO*** estimation. New preload-sensitive parameter of ***PTBC*** is proposed like Eq. (2-32) and (2-33), where the meaning of ***L*1**, ***L*2**, ***R*1**, and ***R*2** is shown in **Figure 2. 7**.

$$PTBC_L = 100\frac{L1}{L1 + L2} \tag{2-32}$$

$$PTBC_R = 100\frac{R1}{R1 + R2} \tag{2-33}$$

As $\boldsymbol{PTBC_L}$ and $\boldsymbol{PTBC_R}$ are divided by (***L*1+*L*2**) or (***R*1+*R*2**), these parameters are independent of the velocity. The principle of the motor current waveform is shown in **Figure 2. 8**.

- Determination of the current level (***CL***): In the case of passive-filling device, ***CL*** is not an important problem, because of the equal ***IVP***. However in the case of active-filling device, ***CL*** must be low, because of the possible current increase by negative-directional ***IVP***. Minimum requirement of ***CL*** is the current consumption by friction and inertia. *In vitro* and *in vivo* test showed that around 0.1 [A] is acceptable (**Figure 2. 9. (b)** is monitoring of the sheep with 28 days survival record. And the consumption of motor current caused by frictional and inertia loss is less than about 0.1 [A].)

Afterload insensitivity means that the ***PTBC*** has little relations with ***AoP*** and ***PAP***. As is apparent in the **Figure 2. 9**, the calculated load remains near zero until the actuator comes in contact with the blood sac and the development of pressure in the pump begins. Especially, from **Figure 2. 9. (b)** and **(c)** which are the case of the lower preload of sacs, i.e., both sacs are partial filled conditions, ***PTBC*** reflects only the information of EDV independent of preload of the opposite sac.

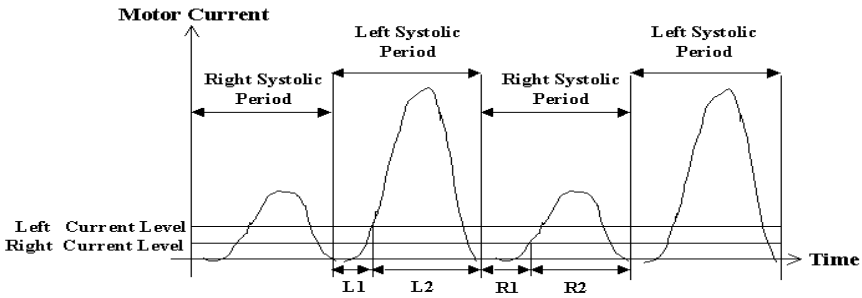

Fig. 2. 7. Typical motor current waveform. $\boldsymbol{PTBC_L}$ = 100***L1***/(***L1***+***L2***), $\boldsymbol{PTBC_R}$ = 100***R1***/(***R1***+***R2***).

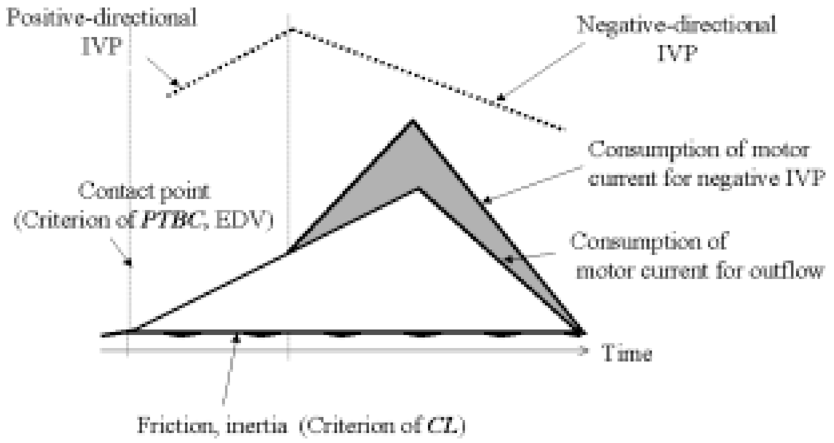

(a)

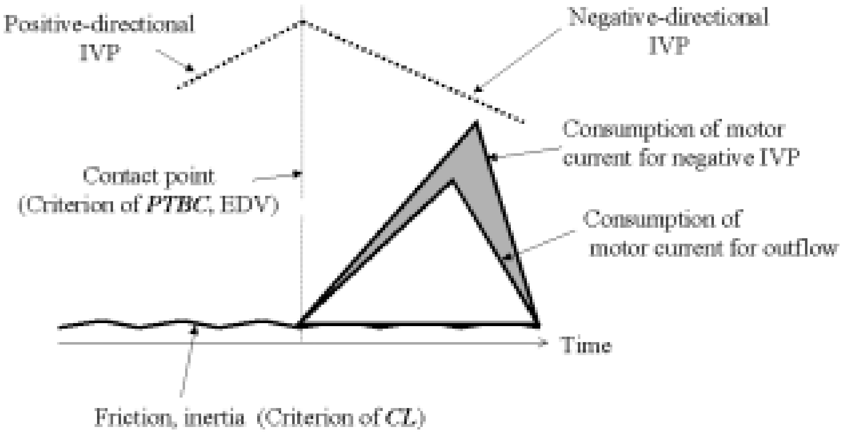

(b)

Fig. 2. 8. Principles of motor current waveform. (a) full fill, (b) partial fill.

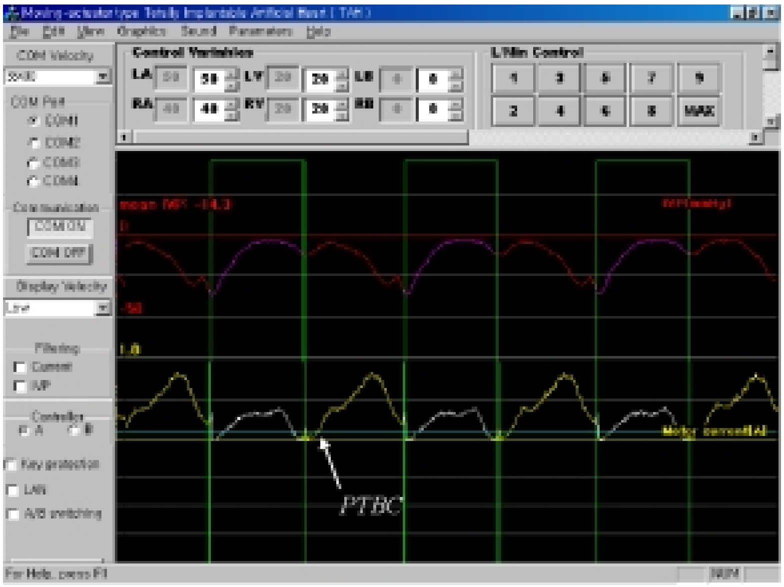

(a)

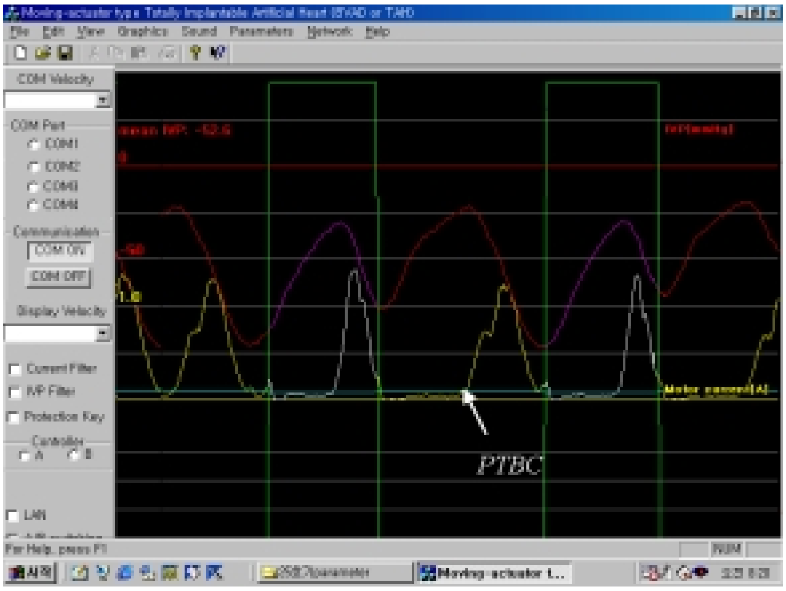

(b)

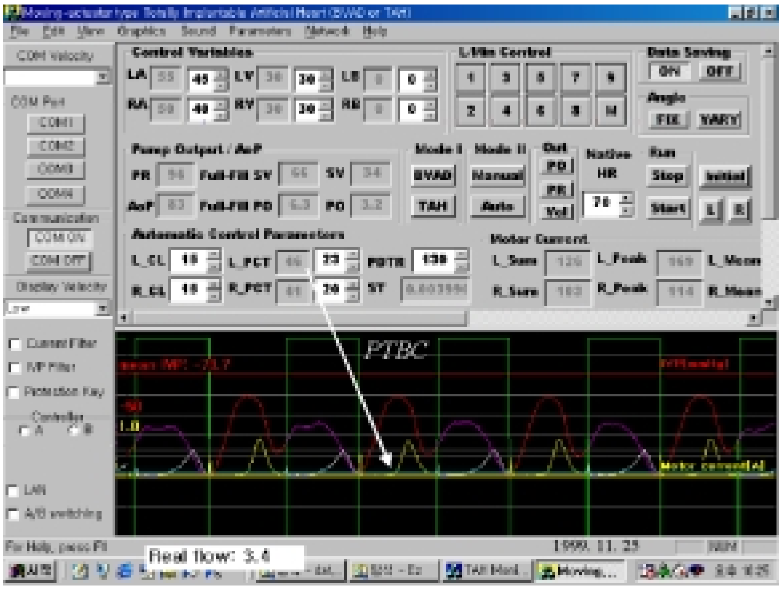

(c)

Fig. 2. 9. Monitoring of motor current (a) *in vitro*: full-fill, (b) *in vivo*: partial-fill (28 days survival), (c) *in vivo*: partial-fill.

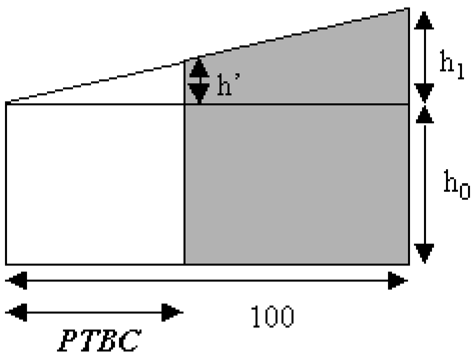

Fig. 2. 10. Filling state of blood sac.

Also, ***PTBC*** can be used for the finding of f_d (***filling state***). The ***PTBC*** is inversely proportional to preload of the ***LAP***. High, middle, and low ***PTBC*** represents that ***LAP*** is low, middle, and high state, respectively. From **Figure 2. 10,** f_d (***filling state***) can be considered like:

$$\begin{aligned} f_d\,(\,filling\ state) &= 1 - \frac{PTBC\left(h_0 + \frac{1}{2}h'\right)}{100\left(h_0 + \frac{1}{2}h_1\right)} \\ &= 1 - \frac{PTBC\left(h_0 + \frac{PTBC}{200}h_1\right)}{100\left(h_0 + \frac{1}{2}h_1\right)} \\ &= 1 - \frac{PTBC\left(c_1 - c_0 SA_R + \frac{PTBC}{200}c_0\left(SA_L + SA_R\right)\right)}{100\left(c_1 + \frac{1}{2}c_0\left(SA_L - SA_R\right)\right)} \end{aligned} \tag{2-34}$$

where

$$h_0 = -c_0 SA_R + c_1 \tag{2-35}$$

and

$$\begin{aligned} h_1 &= (c_0 SA_L + c_1) - h_0 \\ &= c_0\,(SA_L + SA_R) \end{aligned} \tag{2-36}$$

For an active-filling device and by the control, the ***PTBC*** is not dynamically changed. *In vivo* experiences show that the ***PTBC*** is about in the center of the operational range. For $h_1 = h'$ (pusher-plate TAH system of Penn State University) or (h_0+$PTBC \cdot h_1$/200) ≅ (h_0+h_1/2),

$$f_d\,(\,filling\ state) = 1 - \frac{PTBC}{100} \tag{2-37}$$

From Eq. (2-4), (2-31), and (2-34), the SV_L is

$$\begin{aligned}
SV_L &= SV_{L0} \times f_d(\textit{filling state}) \times f_s(mAoP) \\
&= \left(c_0\left(SA_L^2 - SA_R^2\right) + c_1\left(SA_L + SA_R\right)\right) \times \\
&\left(1 - \frac{PTBC\left(c_1 - c_0 SA_R + \frac{PTBC}{200} c_0\left(SA_L + SA_R\right)\right)}{100\left(c_1 + \frac{1}{2} c_0\left(SA_L - SA_R\right)\right)}\right)\left(1 - c_2 mAoP\right)
\end{aligned} \tag{2-38}$$

For $h_1 = h'$ (pusher-plate TAH system of Penn State University) or (h_0+$PTBC \cdot h_1$/200) ≅ (h_0+h_1/2),

$$\begin{aligned}
SV_L &= SV_{L0} \times f_d(\textit{filling state}) \times f_s(mAoP) \\
&= \left(c_0\left(SA_L^2 - SA_R^2\right) + c_1\left(SA_L + SA_R\right)\right)\left(1 - \frac{PTBC}{100}\right)\left(1 - c_2 mAoP\right)
\end{aligned} \tag{2-39}$$

The above equation satisfies '***SV conditions***'.

2. 2. 4. Aortic pressure (*AoP*) estimator

In this dissertation, *energy equilibrium* is used for the development of ***mAoP*** model for MA-BVAD. The internal controller has a motor current sensing system like **Figure. 2. 11**. At first, the consumed input energy is

$$\begin{aligned}
W_{input} &= \int_0^T p(t)dt \\
&= V \int_0^T i(t)dt \\
&\sim a_0 \cdot \left(\sum_0^T i[t] \bullet ST\right)
\end{aligned} \tag{2-40}$$

where $p(t)$, V, $i(t)$, and ST represent the power, voltage, current, and sampling time, respectively. Even if we do not know ST, we can estimate ST from

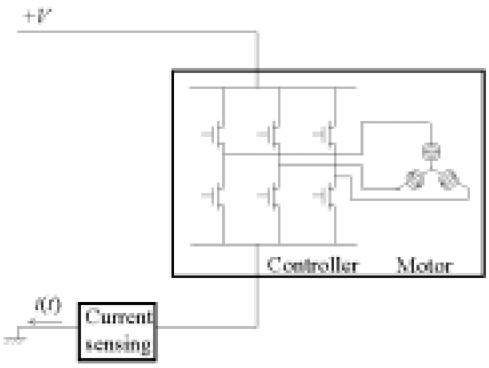

Fig. 2. 11. Sensing of motor current.

$$ST = \frac{60}{Number\ of\ motor\ current\ samples\ per\ cycle \times PR} \tag{2-41}$$

The energy consumed in inertia and ***SV*** is

$$\begin{aligned} W_{load} &= \frac{1}{2}J_M w^2 + \frac{1}{2}J_L v^2 + \int_0^T (AoP(t) - IVP_L(t))Q(t)dt \\ &\sim a_1 w^2 + \sum_0^T (AoP[t] - IVP_L[t])Q[t]ST \\ &\sim a_1 w^2 + (mAoP - mIVP_L) \bullet SV_{L0d} \end{aligned} \tag{2-42}$$

where J_m, J_L, and $Q(t)$ represent the motor inertia, load inertia, and flow rate, respectively. And, $mIVP_L$ represents the mean IVP_L generated in the interventricular space and it is a negative value in general. The counterparts among various systems are summarized in **Table 2. 3**. And the SV_{L0d} is

$$\begin{aligned} SV_{L0d} &= SV_{L0} \times f_d(\,filling\ state) \\ &= \left(c_0\left(SA_L^2 - SA_R^2\right) + c_1\left(SA_L + SA_R\right)\right) \times \\ &\left(1 - \frac{PTBC\left(c_1 - c_0 SA_R + \frac{PTBC}{200}c_0\left(SA_L + SA_R\right)\right)}{100\left(c_1 + \frac{1}{2}c_0\left(SA_L - SA_R\right)\right)}\right) \end{aligned} \tag{2-43}$$

Table 2. 3. Counterparts among various systems.

Translational motion	Rotational motion	Electric circuit	Fluid dynamics
Force $f(t) = ma(t)$ $= m\frac{dv(t)}{dt}$ $= m\frac{d^2x(t)}{dt^2}$	Torque $T(t) = J\alpha(t)$ $= J\frac{dw(t)}{dt}$ $= J\frac{d^2\theta(t)}{dt^2}$	Voltage $V(t)$	Pressure $p(t)$
Power $p(t) = f(t)v(t)$	Power $p(t) = T(t)w(t)$	Power $p(t) = V(t)i(t)$	Power $p(t) = P(t)Q(t)$
Work/energy $w(t) = \int_0^t p(t)dt$ $= \int_0^t f(t)v(t)dt$ $= \int_0^x f(x)dx$	Work/energy $w(t) = \int_0^t p(t)dt$ $= \int_0^t T(t)w(t)dt$ $= \int_0^\theta T(\theta)d\theta$	Work/energy $w(t) = \int_0^t p(t)dt$ $= \int_0^t V(t)i(t)dt$	Work/energy $w(t) = \int_0^t p(t)dt$ $= \int_0^t P(t)Q(t)dt$
or $w(t) = \frac{1}{2}mv(t)^2$	or $w(t) = \frac{1}{2}Jw(t)^2$		
where m: mass $x(t)$: displacement $v(t)$: velocity $a(t)$: accelaration	where J: inertia $\theta(t)$: angular displacement $w(t)$: angular velocity $\alpha(t)$: angulr accelaration	where $i(t)$: current	where $Q(t)$: flow rate

For $h_1 = h'$ (pusher-plate TAH system of Penn State University) or $(h_0+PTBC\cdot h_1/200) \cong (h_0+h_1/2)$,

$$\begin{aligned} SV_{L0d} &= SV_{L0} \times f_d\,(\textit{filling state}) \\ &= \left(c_0\left(SA_L^2 - SA_R^2\right) + c_1\left(SA_L + SA_R\right)\right)\left(1 - \frac{PTBC}{100}\right) \end{aligned} \tag{2-44}$$

Whenever there is motion or tendency of motion between two physical elements, frictional forces exist. The frictional forces encountered in physical systems are usually of a nonlinear nature. The characteristics of the frictional forces between two contacting surfaces often depend on such factors as the composition of the surfaces, the pressure between the surfaces, their relative velocity, and others, so that an exact mathematical description of the frictional force is difficult.

Three different types of friction are commonly used in practical systems: *viscous friction, static friction, and Coulomb friction* [17]. For the rotational motion, the mathematical expression of torque of viscous, static, and Coulomb frictions are Eq. (2-45), (2-46), and (2-47), respectively.

$$T_{f_v}(t) = v\frac{d\theta(t)}{dt} = vw(t) \tag{2-45}$$

$$T_{f_s}(t) = \pm(s)\big|_{\dot{\theta}=0} \tag{2-46}$$

$$T_{f_c}(t) = c\frac{d\theta(t)/dt}{\left|d\theta(t)/dt\right|} = c\frac{w(t)}{\left|w(t)\right|} \tag{2-47}$$

where v, s, c, θ, and w represent the viscous friction constant, static friction constant, Coulomb friction constant, stroke angle, and angular velocity, respectively. Then the total consumption of frictional energy is

$$
\begin{aligned}
W_{friction} &= \int_0^{\theta} T_f(\theta) d\theta \\
&= \int_0^{\theta} \left(T_{f_s}(\theta) + T_{f_c}(\theta) + T_{f_v}(\theta) \right) d\theta \\
&= \int_0^{\theta} (s\delta(\theta) + c + vw(\theta)) d\theta \\
&\sim s + c\theta + vw\theta
\end{aligned}
\qquad (2\text{-}48)
$$

where $\delta(\theta)$ is the delta function. From $W_{input} = W_{load} + W_{friction}$, the final ***mAoP*** is

$$
mAoP - mIVP_L \cong \left. \frac{a_0 (\sum_0^T i[t] \cdot ST) - s - c\theta - vw\theta - a_1 w^2}{SV_{L0d}} \right|_{\theta = SA_L + SA_R, w = Vel_L} \qquad (2\text{-}49)
$$

Similarly, we can set up ***mPAP*** model by using the symmetric characteristics between ***mAoP*** and ***mPAP***, but as the variational range of ***mPAP*** is small compared with ***mAoP*** and as the ***mIVP*** has similar range of ***mPAP***, it is hard to sensitively determine the ***mPAP*** from motor current.

In another view point, and for the comparisons between proposed ***mAoP*** estimation model and that of Penn State University [16], other ***AoP*** estimation model from the *force equilibrium* is introduced like

$$
Pressure \sim Torque - Friction - Acceleration \qquad (2\text{-}50)
$$

$$
Pressure \sim K_T i - Friction - Acceleration \qquad (2\text{-}51)
$$

$$
Pressure \sim K_T \frac{V - K_b w}{R} - Friction - Acceleration \qquad (2\text{-}52)
$$

$$
Pressure \sim K_T \frac{V - K_b w}{R} - K_1 w - K_2 w^2 - K_3 w^2 - K_4 \qquad (2\text{-}53)
$$

where $\boldsymbol{K_T}$, $\boldsymbol{I}$, $\boldsymbol{V}$, $\boldsymbol{K_b}$, $\boldsymbol{w}$, $\boldsymbol{R}$, $\boldsymbol{K_1}$, $\boldsymbol{K_2}$, $\boldsymbol{K_3}$, and $\boldsymbol{K_4}$ represent the motor's torque constant, the motor current, voltage, the back electromotive force constant, the angular velocity, resistance, viscous losses (motor, bearings, pump, and outlet valve), additional viscous loss in the outlet valve, the combined inertia (motor, mechanism, and blood), and the constant friction not dependent upon speed or load, respectively.

2. 2. 5. Tuning of model's constants

For the adaptation of the model's constants, various methods are known, and the famous and simple, but robust and good capable algorithm is the *pseudoinverse* and *least mean square* (LMS) algorithm ones. Pseudoinverse method is the least square algorithm. Let **A** denote a $\boldsymbol{K}$-by-$\boldsymbol{M}$ matrix ($\boldsymbol{K} > \boldsymbol{M}$), and we assume that the rank $\boldsymbol{W}$ equals $\boldsymbol{M}$ so that the inverse matrix $(\mathbf{A}^{\mathrm{T}}\mathbf{A})^{-1}$ exists. Where **T** denotes the transpose of a matrix. Then the *pseudoinverse* or the *Moore-Penrose generalized inverse* of the matrix **A** is defined by $\mathbf{A}^{+}$ like

$$\mathbf{A}^{+} = (\mathbf{A}^{\mathbf{T}}\mathbf{A})^{-1}\mathbf{A}^{\mathbf{T}} \tag{2-54}$$

The detailed proof can be seen in pp. 524-525 of [18].

For the constant estimation of $\boldsymbol{PO}$ model with given $\boldsymbol{n}$ data set, we can setup matrix like

$$\begin{bmatrix} \boldsymbol{SV}_0[1] \\ \boldsymbol{SV}_0[2] \\ \vdots \\ \boldsymbol{SV}_0[\boldsymbol{n}] \end{bmatrix} = \begin{bmatrix} (\boldsymbol{SA}_L^2 - \boldsymbol{SA}_R^2)[1] & (\boldsymbol{SA}_L + \boldsymbol{SA}_R)[1] \\ (\boldsymbol{SA}_L^2 - \boldsymbol{SA}_R^2)[2] & (\boldsymbol{SA}_L + \boldsymbol{SA}_R)[2] \\ \vdots & \\ (\boldsymbol{SA}_L^2 - \boldsymbol{SA}_R^2)[\boldsymbol{n}] & (\boldsymbol{SA}_L + \boldsymbol{SA}_R)[\boldsymbol{n}] \end{bmatrix} \begin{bmatrix} \boldsymbol{c}_0 \\ \boldsymbol{c}_1 \end{bmatrix} \tag{2-55}$$

By applying pseudoinverse,

$$\begin{bmatrix} c_0 \\ c_1 \end{bmatrix} = \begin{bmatrix} (SA_L^2 - SA_R^2)[1] & (SA_L + SA_R)[1] \\ (SA_L^2 - SA_R^2)[2] & (SA_L + SA_R)[2] \\ \vdots & \\ (SA_L^2 - SA_R^2)[n] & (SA_L + SA_R)[n] \end{bmatrix}^{+} \begin{bmatrix} SV_0[1] \\ SV_0[2] \\ \vdots \\ SV_0[n] \end{bmatrix} \tag{2-56}$$

For the constant estimation of ***AoP*** model with given ***n*** data set,

$$\begin{bmatrix} (mAoP - mIVP)[1] \\ (mAoP - mIVP)[2] \\ \vdots \\ (mAoP - mIVP)[n] \end{bmatrix} = \begin{bmatrix} (\sum_0 i[t][1] \cdot ST) & (-1) & (-\theta[1]) & (-w[1]\theta[1]) & (-w[1]^2) \\ (\sum_0 i[t][2] \cdot ST) & (-1) & (-\theta[2]) & (-w[2]\theta[2]) & (-w[2]^2) \\ & & \vdots & & \\ (\sum_0 i[t][n] \cdot ST) & (-1) & (-\theta[n]) & (-w[n]\theta[n]) & (-w[n]^2) \end{bmatrix} \begin{bmatrix} a_0 \\ s \\ c \\ v \\ a_1 \end{bmatrix} \tag{2-57}$$

By applying pseudoinverse,

$$\begin{bmatrix} a_0 \\ s \\ c \\ v \\ a_1 \end{bmatrix} = \begin{bmatrix} (\sum_0 i[t][1] \cdot ST) & (-1) & (-\theta[1]) & (-w[1]\theta[1]) & (-w[1]^2) \\ (\sum_0 i[t][2] \cdot ST) & (-1) & (-\theta[2]) & (-w[2]\theta[2]) & (-w[2]^2) \\ & & \vdots & & \\ (\sum_0 i[t][n] \cdot ST) & (-1) & (-\theta[n]) & (-w[n]\theta[n]) & (-w[n]^2) \end{bmatrix}^{+} \begin{bmatrix} (mAoP - mIVP)[1] \\ (mAoP - mIVP)[2] \\ \vdots \\ (mAoP - mIVP)[n] \end{bmatrix} \tag{2-58}$$

Eq. (2-56) and (2-58) are batch processing, so these method can be used only in *off-line* situation. For *on-line* application, recursive least-squares (RLS) algorithm can be used.

2. 3. Pump Output Control of MA-BVAD

There are three kinds of control modes in the VAD system: fixed ***PR*** mode, fixed ***SV*** mode (fixed volume and variable rate mode, full-to-empty mode, pump-on-full mode, preload-sensitive mode), and synchronous mode (synchronized counterpulsation to the native heart by sensing the electrocardiogram R wave). In this dissertation, four kinds of ***PO*** control modes were studied: 1) Fixed ***PR*** control, 2) fixed ***SV*** control, 3) ***HR***-based control, and 4) total assist control. 1) and 2) are the common control methodologies in the VAD system. The third one is the modified version of synchronous control. At last, the fourth was studied for the preparation against heart attack. When a heart attack is occurred, the controller must switch from biventricular assist control mode to the total assist control mode. This mode is similar to the TAH control, and the MA-BVAD can be operated like TAH. The differences between the biventricular assist control mode and total assist control mode is:

- Left/right flow balance is not a critical factor for BVAD control, because of the native heart function.

Developed control algorithms were a rule-based control system, i.e., its form is 'If ~, then ~'. And, the constructed control algorithms have a simple structure.

2. 3. 1. Fixed *PR* control

Fixed ***PR*** control mode is widely used in the VAD system because of its simplicity and acceptable ***PO*** control. The rule-base for fixed ***PR*** control is as follows:

- ***Rule 1:*** If ***PR*** > target ***PR***, then the $\boldsymbol{Vel_L}$ is decreased by one and the $\boldsymbol{Vel_R}$ is changed to be 100*$\boldsymbol{Vel_L}$/***PDTR***.
- ***Rule 2:*** If ***PR*** < target ***PR***, then the $\boldsymbol{Vel_L}$ is increased by one and the $\boldsymbol{Vel_R}$ is changed to be 100*$\boldsymbol{Vel_L}$/***PDTR***.

2. 3. 2. Fixed *SV* control

The left ventricular filling state is determined from the difference between the $\boldsymbol{PTBC_L}$ and the target $\boldsymbol{PTBC_L}$ (LMA mode). As noninvasive input control parameters, there are the ***IVP*** and the motor current for MA-BVAD. Motor current is more favorite choice than the ***IVP*** because ***IVP*** reflects the dynamic inflow state not the EDV. Left and right stroke angle ($\boldsymbol{SA_L}$, $\boldsymbol{SA_R}$), velocity ($\boldsymbol{Vel_L}$, $\boldsymbol{Vel_R}$), and the brake time ($\boldsymbol{BT_L}$, $\boldsymbol{BT_R}$) are possible control parameters for MA-BVAD. The $\boldsymbol{BT_L}$ and $\boldsymbol{BT_R}$ are not used in this research because of their minor effect on the performance of control and complexity of control algorithm. The $\boldsymbol{Vel_L}$ is fixed to produce the desired middle ***PR*** together with the same $\boldsymbol{Vel_R}$. Even if $\boldsymbol{Vel_L}$ and $\boldsymbol{Vel_R}$ can be changed, the fixed $\boldsymbol{Vel_L}$ makes the control system simpler and the $\boldsymbol{PTBC_L}$ more reliable.

- ***Rule 1:*** If filling is bad ($\boldsymbol{PTBC_L}$ > target $\boldsymbol{PTBC_L}$), the $\boldsymbol{Vel_R}$ is decreased by the difference between $\boldsymbol{PTBC_L}$ and target $\boldsymbol{PTBC_L}$.
- ***Rule 2:*** If filling is good ($\boldsymbol{PTBC_L}$ < target $\boldsymbol{PTBC_L}$), the $\boldsymbol{Vel_R}$ is increased by the difference between $\boldsymbol{PTBC_L}$ and target $\boldsymbol{PTBC_L}$.

These rules permit the controller to produce the ventricular assist flow proportional to the left preload (LMA mode). Similar studies of other research groups also adopted the LMA mode [34]. Two limiters inhibit the undesirable high deviation of the control action

- ***Limiter 1:*** The ***PR*** must be inside between the minimum ***PR*** and the maximum ***PR***
- ***Limiter 2:*** Low and high damping levels prevent the extreme velocity action.

If ***limiter 1*** is not necessary, the operator can set the minimum ***PR*** and the maximum ***PR*** to be extreme case of 0 and 200, respectively, or one of them can be neglected.

2. 3. 3. *HR*-based control

One of mechanisms of the native heart control is the *feedback control* acting through the *central nervous system*. By this mechanism and with the *sympathetic* and *parasympathetic* nerves, the natural heart increases or decreases the ***HR***. We can infer the flow of body demand from this information of ***HR***. In the case of TAH, the ***HR*** information is impractical, even if there was a trial to use the P wave as an input control parameter in the remnant atria [36].

To maximize the ***SV*** with synchronous counterpulsation (by sensing the electrocardiogram R wave) is best in the perspective of maximizing VAD output, left ventricular decompression, and blood contact surface cleansing. But the requirement of development of this control system becomes more complex than the other control modes. Furthermore, as the present MA-BVAD is active-filling device, high synchronous and high ***PR*** have the possibility of suction problem.

Considering the above points, the following rule and limiter were proposed for the ***HR***-based control mode of biventricular assist.

- ***Rule 1:*** The ***PR*** is controlled to be linearly proportional to the ***HR***
- ***Limiter 1:*** The ***PR*** must be inside between minimum ***PR*** and maximum ***PR***

The tracking algorithm for the target ***PR*** is the same as the fixed ***PR*** control. If ***limiter 1*** is not necessary, the operator can set the minimum ***PR*** and maximum ***PR*** to be extreme case of 0 and 200, respectively, or one of them can be neglected.

2. 3. 4. Total assist control

As the preperation against heart attack, alternative preload-sensitive total assist control algorithm using ***PTBC*** was developed in this section. The targeted mechanism of control is to mimic the *Frank-Starling mechanism*.

Proposed strategy for the left/ right balanced output control is:

- Relative left and right diastolic time (percent diastolic filling time ratio, ***PDTR*** = 100$\boldsymbol{Vel_L}/\boldsymbol{Vel_R}$.) proposed by Kim [2]. This is the utilization of the control capability of the relationship between ***LAP*** and ***RAP*** by the choice of the relative left and right diastolic speeds.
- Longer $\boldsymbol{SA_L}$ than $\boldsymbol{SA_R}$: After appropriate air volume adjustment for small passive filling, determination of $\boldsymbol{SA_R}$ (most cases are about 90 % of the left side) with the fixed maximum $\boldsymbol{SA_L}$ follows. This permits the pump to produce the highest efficiency and washout effect (minimize the likelihood of generation of thrombosis and hemolysis by lowering residual volume and ***PR***). Fixed ***SA*** makes the hemodynamic estimation and automatic control simple.
- Greater left ventricular volume than right one.
- Compliance window for the compensation of left and right volume.

Nowadays, the *variable rate* control systems is popular (Proposed algorihm, Penn State TAH, Baylor College TAH, Helmholtz Institute TAH). This mode of TAH function maximizes pump efficiency by providing the maximum ***SV*** (full-fill governing principle) with each systolic phase and by varying the ***PR*** to meet metabolic demands. Next, the proposed automatic control algorithm utilizes two schemes for the preload-sensitive control as follows [45]:

- Intrinsic control (small passive filling): Air between the ventricles with detached actuator from the ventricles.
- Extrinsic control (active preload sensitive control): ***PTBC*** between actuator and ventricle is inverse proportional to the preload (***LAP***, ***RAP***). By controlling to produce the ***PTBC*** to be a predetermined setting value, TAH can mimic the natural heart, i.e., the physiological demand is estimated from ***PTBC***. A predetermined EDV acts as a trigger to initiate systole by keeping the ***PTBC*** constant.

The rule-base is as follows:

- ***Rule 1:*** If left ‘***or’*** right filling is bad ($\boldsymbol{PTBC_L}$ > target $\boldsymbol{PTBC_L}$ ***‘or’*** $\boldsymbol{PTBC_R}$ > target $\boldsymbol{PTBC_R}$), then the $\boldsymbol{Vel_L}$ is decreased by one, and $\boldsymbol{Vel_R}$ is changed to be 100*$\boldsymbol{Vel_L}$/***PDTR***.
- ***Rule 2:*** If left ***‘and’*** right filling is good ($\boldsymbol{PTBC_L}$ < target $\boldsymbol{PTBC_L}$ ***‘and’*** $\boldsymbol{PTBC_R}$ < target $\boldsymbol{PTBC_R}$), then the $\boldsymbol{Vel_L}$ is increased by one, and $\boldsymbol{Vel_R}$ is changed to be 100*$\boldsymbol{Vel_L}$/***PDTR***.

The ***PR*** is computed continuously, and when the ***PR*** falls below the minimum ***PR***, the control is automatically switched to the internal fixed rate mode of minimum ***PR***:

- ***Limiter 1:*** If the $\boldsymbol{Vel_L}$ lower than the minimum $\boldsymbol{Vel_L}$, then the $\boldsymbol{Vel_L}$ is increased by one, and $\boldsymbol{Vel_R}$ is changed to be 100*$\boldsymbol{Vel_L}$/***PDTR***.

In **Figure 2. 12**, the block diagram of the overall preload-sensitive control is shown. This algorithm is executed every regular cyclic period (in general, three beats). The basic control scheme is ‘*when the inflow to the sac is decreased, the* ***PR*** *decreases until the contacting point between actuator and sac is moved to the setting threshold value and vice versa (proportional output with RAP: Starling law)*’. Proposed algorithm can be characterized by ‘LMA emphasized LMA+RMA control'.

- As our MA-BVAD has the characteristics of active-filling, not only $\boldsymbol{PTBC_L}$ but also $\boldsymbol{PTBC_R}$ must be considered simultaneously because of the possibility of right atrium's collapse from suction effect (LMA+RMA control)
- The sensitivity of target $\boldsymbol{PTBC_L}$ must be higher than that of target $\boldsymbol{PTBC_R}$ because ***LAP*** control is more important than ***RAP*** control (Right ventricle is monitored whether there is suction or not, LAM emphasized control).

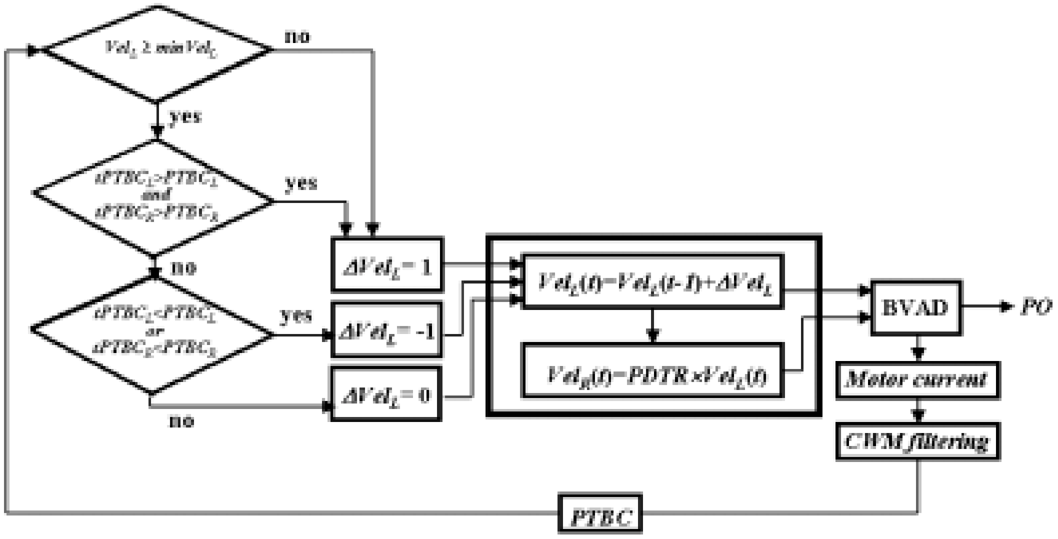

Fig. 2. 12. Block diagram of the total assist control. ***tPTBC***: target ***PTBC***.

2. 3. 5. Common considerations

As the physiological system produces delayed response, the control action, in general, must be triggered every a few cycles. And, all the parameters must be processed by running mean filters for the exclusion of the respiration effect and some variation caused by noise and so on.

- *Cyclic beats* for the control action.
- *Running mean filters* to eliminate the external disturbances such as noise and respiration effect.

3. RESULTS

At first, the performance of a *CWM filter* was analyzed in **Section 3. 1**. After that, the developed ***PO*** and ***AoP*** *estimators* and the ***PO*** *control algorithms* were verified in **Section 3. 2** and **3. 3**, respectively.

3. 1. Performance of a CWM Filter for Noise Suppression

Figure 3. 1. (a) is the original motor current signal. We can see that there are impulsive noisy terms. **Figure 3. 1. (b)** is the motor current signal filtered by a CWM filter (side-length $\boldsymbol{L}$ = 2, central weight $\boldsymbol{w}$ = 1). For comparison, filtered motor current signals by a median filter ($\boldsymbol{L}$ = 2) and a mean filter ($\boldsymbol{L}$ = 2) are shown in **Figure 3. 1. (c) and (d)**. As expected, mean filter is not good enough to overcome the impulsive noise problem. Next, for lower cost of operation we considered the filter with $\boldsymbol{L}$ = 1. In this case, CWM filter and the median filter have the same structure because $\boldsymbol{w}$ = 0 for $\boldsymbol{L}$ = 1 in CWM filter. **Figure 3. 1. (e)** and **(f)** are the results of these filters. In the case of another noninvasive signal of ***IVP***, the similar experimental results were gathered and shown in **Figure 3. 2**. We can see that CWM filter ($\boldsymbol{L}$ = 2, $\boldsymbol{w}$ = 1) is the appropriate filter for the motor current and the ***IVP*** signals in the perspective of detail preserving and waveform. In the **Appendix**, the C program source of a CWM filter is presented.

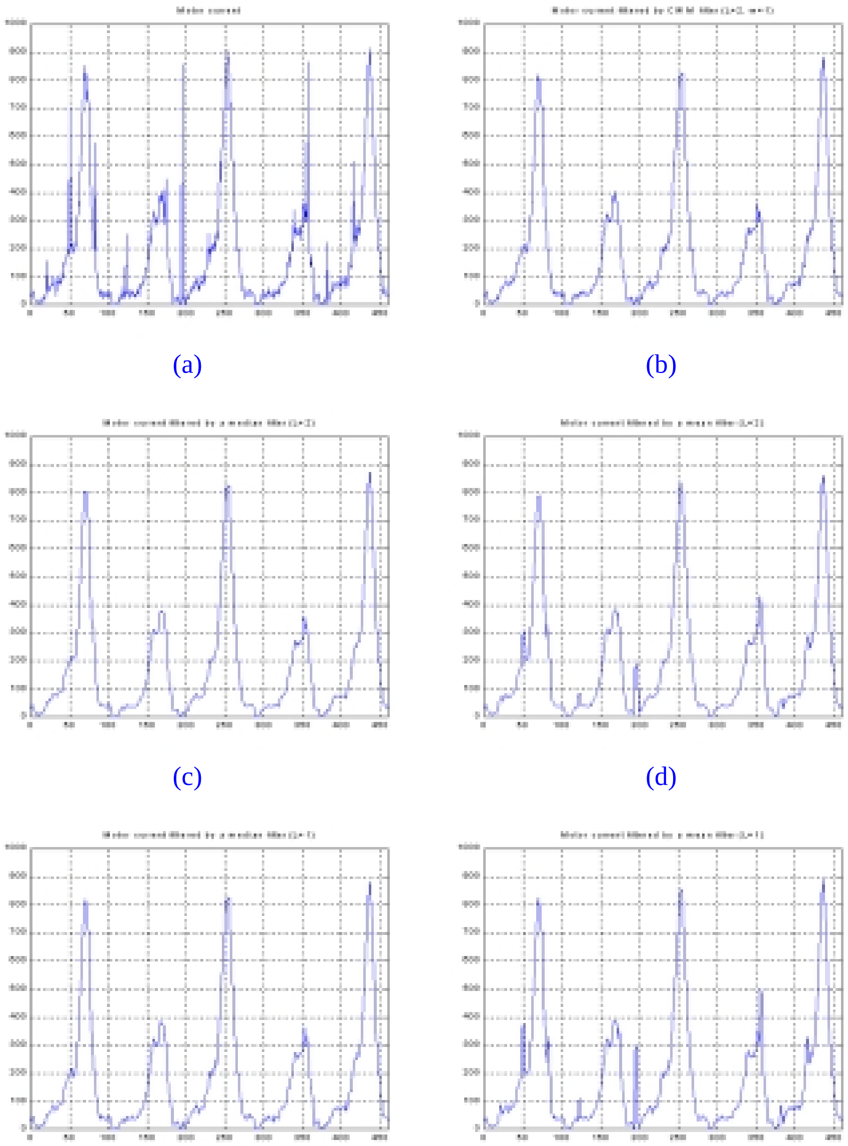

(a) (b) (c) (d) (e) (f)

Fig. 3. 1. Motor current and filtered signals. (a) Original motor current signal contaminated by impulsive noise, (b) motor current signal filtered by a CWM filter (***L*** = 2, ***w*** = 1), (c) motor current signal filtered by a median filter (***L*** = 2), (d) motor current signal filtered by a mean filter (*L* = 2), (e) motor current signal filtered by a median filter (***L*** = 1), (f) motor current signal filtered by a mean filter (***L*** = 1).

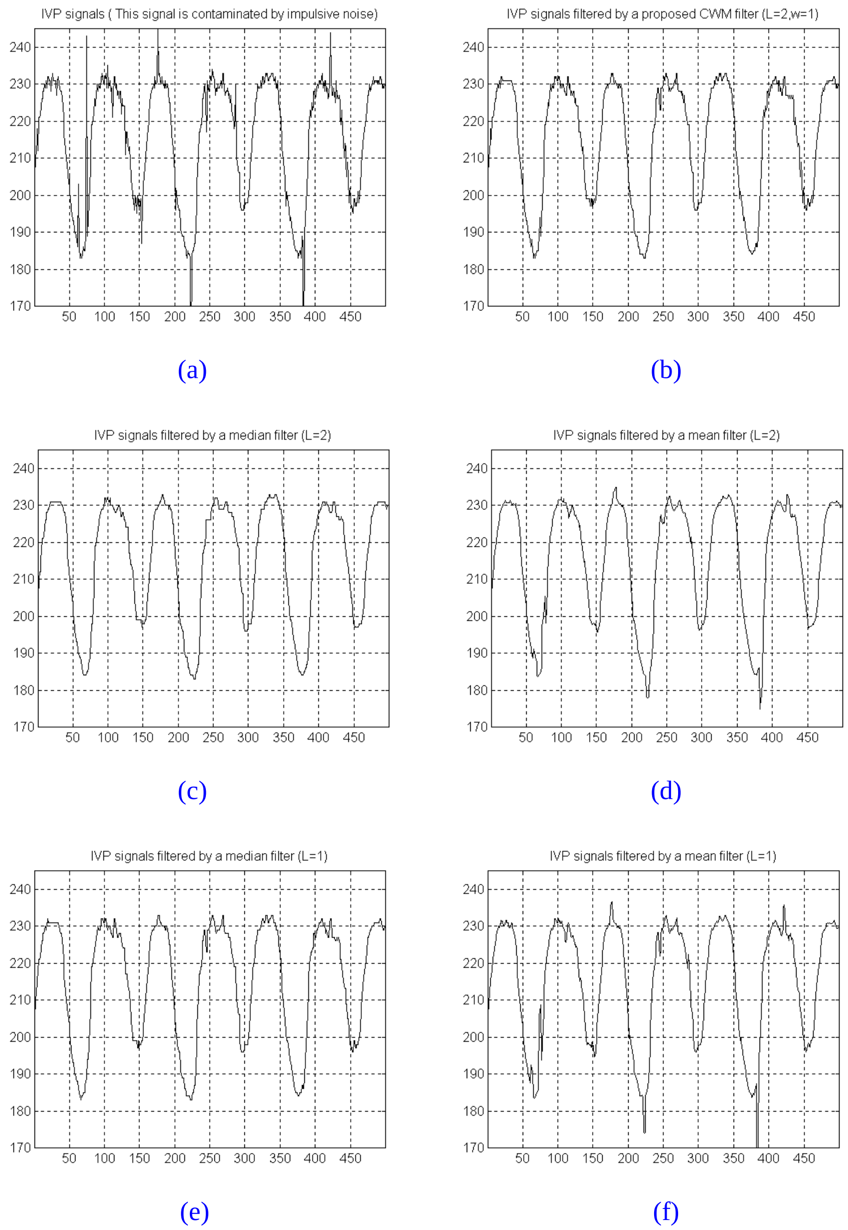

Fig. 3. 2. ***IVP*** signal and filtered signals. (a) Original ***IVP*** signal contaminated by impulsive noise, (b) ***IVP*** signal filtered by a CWM filter ($\boldsymbol{L}$ = 2, $\boldsymbol{w}$ = 1), (c) ***IVP*** signal filtered by a median filter ($\boldsymbol{L}$ = 2), (d) ***IVP*** signal filtered by a mean filter (L = 2), (e) ***IVP*** signal filtered by a median filter ($\boldsymbol{L}$ = 1). (f) ***IVP*** signal filtered by a mean filter ($\boldsymbol{L}$ = 1).

3. 2. *PO* and *AoP* Models

Pseudoinverse is an *one-pass* algorithm. Another method of least mean square (LMS) algorithm is a *stochastic gradient algorithm*, i.e., LMS algorithm requires many recursion. Previous studies showed that LMS algorithm has a rather high sensitivity of initial adaptation ratio and other parameters [19][20]. Here, pseudoinverse is utilized to find the developed ***PO*** and ***AoP*** model's constants from the *in vitro* data. Look-up-table (LUT) for ***PO*** estimator is shown in **Table 3. 1** and the corresponding plot is shown in **Figure 3. 4**. The LUT is acquired by measuring the residual volume in the blood sac using a syringe. From Eq. (2-31), the left and right full-fill/full-out stroke volume ($\boldsymbol{SV}_0$) are

$$\boldsymbol{SV}_{\boldsymbol{L}0} = \boldsymbol{c}_{\boldsymbol{L}0}(\boldsymbol{SA}_{\boldsymbol{L}}^2 - \boldsymbol{SA}_{\boldsymbol{R}}^2) + \boldsymbol{c}_{\boldsymbol{L}1}(\boldsymbol{SA}_{\boldsymbol{L}} + \boldsymbol{SA}_{\boldsymbol{R}}) \quad (3\text{-}1)$$

and

$$\boldsymbol{SV}_{\boldsymbol{R}0} = \boldsymbol{c}_{\boldsymbol{R}0}(\boldsymbol{SA}_{\boldsymbol{R}}^2 - \boldsymbol{SA}_{\boldsymbol{L}}^2) + \boldsymbol{c}_{\boldsymbol{R}1}(\boldsymbol{SA}_{\boldsymbol{R}} + \boldsymbol{SA}_{\boldsymbol{L}}) \quad (3\text{-}2)$$

From Eq. (3-1) and (3-2), the matrix equations of $\boldsymbol{SV}_L$ and $\boldsymbol{SV}_{\boldsymbol{R}}$ for constant's estimation are

$$\begin{bmatrix} 20 \\ 28 \\ 36 \\ 47 \end{bmatrix} = \begin{bmatrix} -2500 & 50 \\ -2400 & 60 \\ -1600 & 80 \\ 0 & 100 \end{bmatrix} \begin{bmatrix} \boldsymbol{c}_{\boldsymbol{L}0} \\ \boldsymbol{c}_{\boldsymbol{L}1} \end{bmatrix} \quad (3\text{-}3)$$

and

$$\begin{bmatrix} 8 \\ 12 \\ 21 \\ 39 \end{bmatrix} = \begin{bmatrix} -2500 & 50 \\ -2400 & 60 \\ -1600 & 80 \\ 0 & 100 \end{bmatrix} \begin{bmatrix} \boldsymbol{c}_{\boldsymbol{R}0} \\ \boldsymbol{c}_{\boldsymbol{R}1} \end{bmatrix} \quad (3\text{-}4)$$

By using the pseudoinverse, c_{L0} and c_{L1} are found to be 0.0008 and 0.4705, respectively. Mean error of estimated SV_{L0} is 0.925 cc. Similarly, c_{R0} and c_{R1} are found to be 0.0047 and 0.3813. Mean absolute error of estimated PO_{R0} is 3.5 cc. Three dimensional plot of the simplified SV_0 model is shown in **Figure 3. 4**. **Figure 3. 4 and 2. 3** have very similar three-dimensional form, except the magnitude of the left and right SV_0. This may stem from the fact that the flexible blood sac is reshaped and blood is displaced radially as shown in **Figure 2. 5**. From above results, we can conclude that the simplified SV_0 model is superior to geometric SV_0 one, in the perspective of simplicity and accuracy. The results were simulated by Matlab 6.0.

LUT for ***mAoP*** estimator is shown in **Table 3. 2** and the corresponding plot is shown in **Figure 3. 5**. By using the pseudoinverse, the a_0, s, c, v, and a_1 are found to be 0.43974, 0.6940, 0.0067, 0.000024841, and 0.00000028545, respectively. The mean absolute error of estimated ***mAoP*** is 5.4 [mmHg]. Here, motor current is converted from analog to digital value and uncalibrated.

Table 3. 1. Determination of SV model's constants. Mean estimated error of SV_{L0} and SV_{R0} are 0.925 cc and 3.5 cc, respectively.

Position of actuator	SV_{L0}	Maximum SV_{L0} – SV_{L0} = 91 – SV_{L0}	Estimated SV_{L0}	SV_{R0}	Maximum SV_{R0} – SV_{R0} = 80 – SV_{R0}	Estimated SV_{R0}
SA_{R0} = 50	86	0	.	43	**39**	**36.3**
SA_{R0} = 30	80	6	.	61	**21**	**21.5**
SA_{R0} = 10	76	10	.	68	**12**	**15.7**
SA_{R0} = SA_{L0} = 0	66	**20**	**21.5**	74	**8**	**11.8**
SA_{L0} = 10	58	**28**	**26.2**	79	3	.
SA_{L0} = 30	50	**36**	**36.3**	81	1	.
SA_{L0} = 50	39	**47**	**47.1**	82	0	.

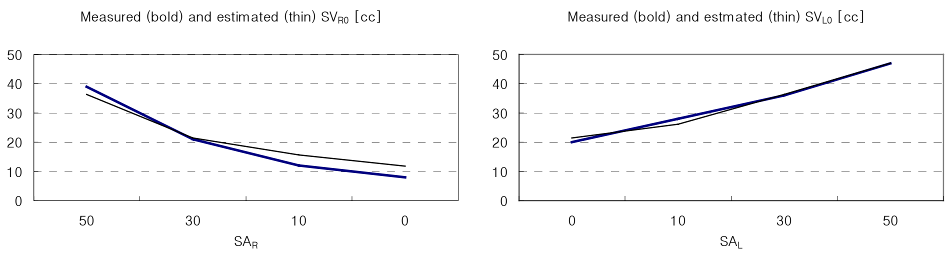

(a) (b)

Fig. 3. 3. Graphical display of **Table 3. 1**. (a) SV_{R0}, (b) SV_{L0}.

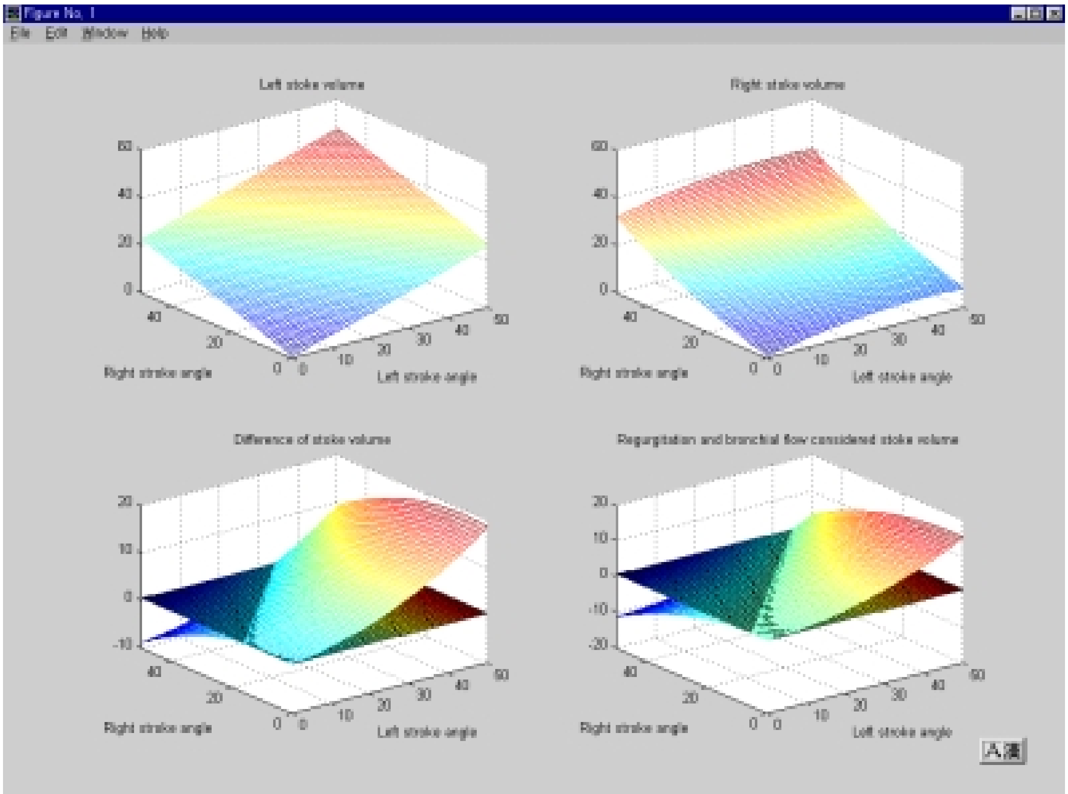

Fig. 3. 4. Simplified SV_0. (a) three dimensional plot, (b) SV_{R0}, (c) SV_{L0}.

Table 3. 2. Determination of ***mAoP*** estimator's constants. ***Vel***$_R$ is 60, ***mIVP*** was set 20 mmHg. Mean estimated error is 5.4 mmHg.

mAoP [mmHg]	***SA***$_L$, ***SA***$_R$	***Vel***$_L$	Left Current Sum	Estimated geometric ***SV***$_0$	Estimated ***mAoP***
140	50, 30	80	490	36.6	**134**
140	50, 30	40	445	36.6	**137**
140	50, 30	60	485	36.6	**144**
100	50, 30	80	425	38.3	**97**
100	50, 30	40	355	38.3	**89**
100	50, 30	60	420	38.3	**107**
70	50, 30	80	390	39.6	**78**
70	50, 30	40	305	39.6	**63**
70	50, 30	60	370	39.6	**81**

mAoP [mmHg]	***SA***$_L$, ***SA***$_R$	***Vel***$_L$	Left Current Sum	Estimated geometric ***SV***	Estimated ***mAoP***
140	50, 50	80	560	41.8	**131**
140	50, 50	40	535	41.8	**148**
140	50, 50	60	540	41.8	**137**
100	50, 50	80	495	43.7	**98**
100	50, 50	40	445	43.7	**104**
100	50, 50	60	465	43.7	**99**
70	50, 50	80	440	45.2	**73**
70	50, 50	40	355	45.2	**65**
70	50, 50	60	410	45.2	**74**

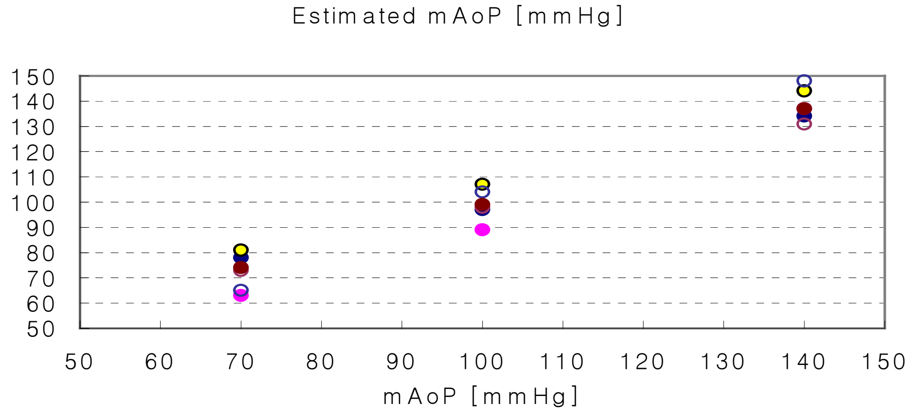

Fig. 3. 5. Graphical display of **Table 3. 2**.

Results of *in vitro* and *in vivo* test are shown in **Figure 3. 6**. As the constants were adjusted by the mechanical flow meter, but the recorded data were gathered by an ultrosonic flowmeter, the estimated ***PO*** was underestimated by a DC drift. Without the effect of DC drift, the general results show very good performance, and the error is lower than 0.5 Liter/min. Graphs (c) and (d) are the cases of constant increase of flow, and (b) is the case of ***mAoP*** estimator. We can verify no severe error in the BVAD's operational range of 50 – 120 [mmHg].

Figure 3. 6. (e) is the trend of estimated ***mAoP*** for 8 days just before the pump weaning. The control parameters were (SA_L, SA_R) = (57, 57), (Vel_L, Vel_R) = (29, 29), (BT_L, BT_R) = (0, 0). The CL_L and CL_R were set 20 and 15, respectively, and the ***PR*** was about 81. From this *in vivo* test, we found there were great gaps between *in vitro* and *in vivo* situations, so ***mAoP*** model's constants were changed heuristically. The real catheter line for the ***mAoP*** measurement was clogged and the reference pressure level was changed by the animal's posture (standing or supine). So, the comparisons between the real ***mAoP*** and the estimated ***mAoP*** cannot be executed, but the general results were acceptable. The real ***mAoP*** and ***mPAP*** maintained at about 75-100 mmHg and 10-20mmHg, respectively. The value was changed by the animal's body posture (standing or supine), neck posture (eating or looking up), etc. This result showed that ***mAoP*** dependent automatic BVAD control is not reasonable, because of the sensitivity of ***mAoP*** depending on the animal's body posture.

As the estimated ***PO*** and ***mAoP*** were processed by running mean filter, the delayed effect cannot be eliminated.

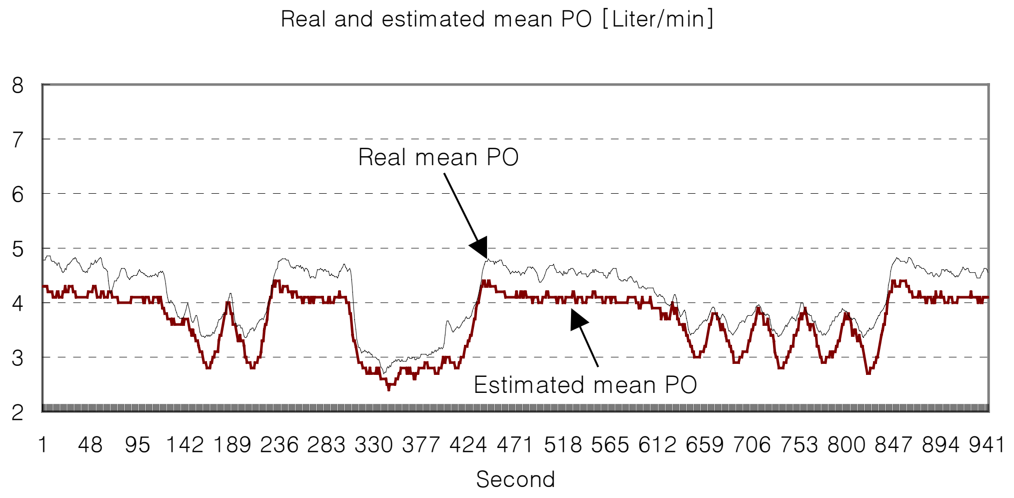
Real and estimated mean PO [Liter/min]
Real mean PO
Estimated mean PO
8
7
6
5
4
3
2
1 48 95 142 189 236 283 330 377 424 471 518 565 612 659 706 753 800 847 894 941
Second

(a)

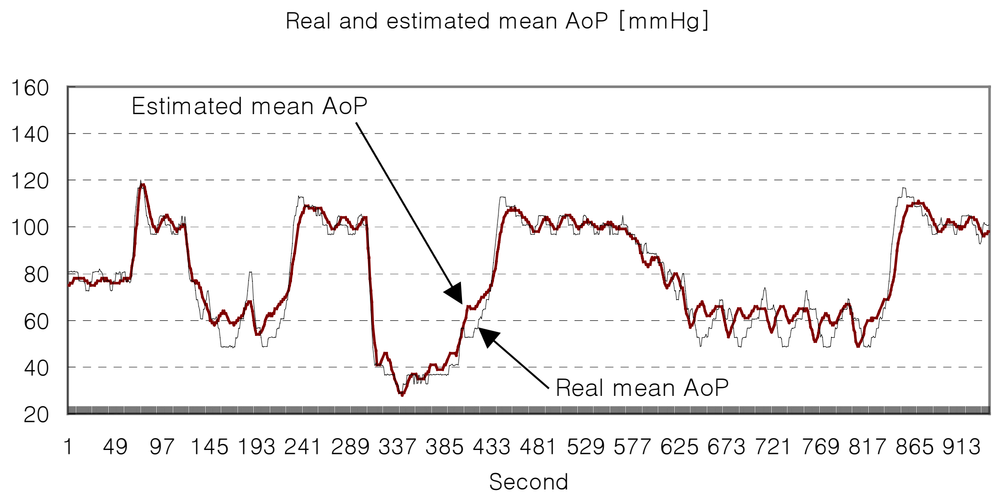
Real and estimated mean AoP [mmHg]
Estimated mean AoP
Real mean AoP
160
140
120
100
80
60
40
20
1 49 97 145 193 241 289 337 385 433 481 529 577 625 673 721 769 817 865 913
Second

(b)

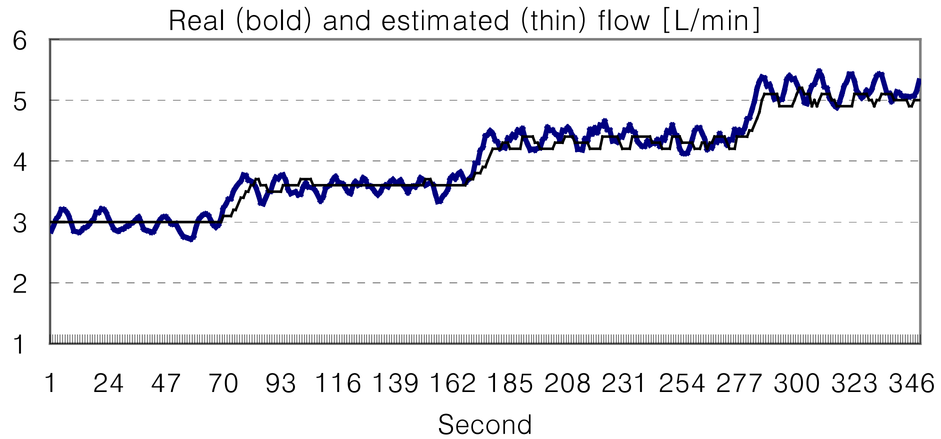
Real (bold) and estimated (thin) flow [L/min]
6
5
4
3
2
1
1 24 47 70 93 116 139 162 185 208 231 254 277 300 323 346
Second

(c)

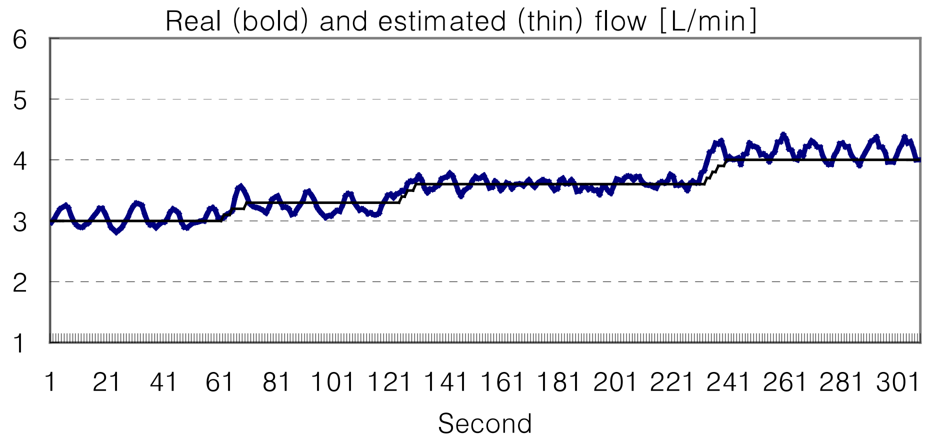
Real (bold) and estimated (thin) flow [L/min]
6
5
4
3
2
1
1 21 41 61 81 101 121 141 161 181 201 221 241 261 281 301
Second

(d)

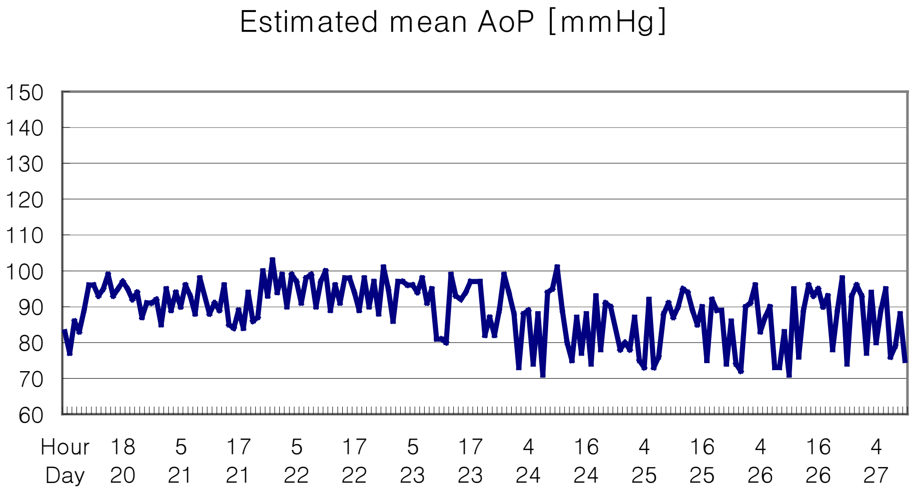

(e)

Fig. 3. 6. *In vitro* and *in vivo* performance test of ***PO*** and ***AoP*** estimators. (a), (b), (c) and (d) *in vitro* test, (e) *in vivo* test of ***AoP*** estimator.

3. 3. *In Vitro* and *In Vivo* Experiments of Developed Control Algorithms

The control system consists of a microcontroller-based (Intel 80C196) internal controller and an external controller (IBM compatible PC). The internal controller performs: (1) brushless DC motor commutation, (2) position and velocity control of the motor according to the physiological control algorithm, and (3) communication with the external controller. The external controller communicates with the internal controller via an RS-232 serial communication protocol. The physician will use this device to monitor the status of the implanted component, change operational mode, and store all data. The automatic control algorithm is implemented as software in the external controller. All parameters related with motor current are analog to digial converted and uncalibrated.

Figure 3. 7 is the *in vitro* test equipment for the biventricular assist controls. The *in vitro* equipments for biventricular assist control modes are composed of the simulated atrium for measuring and changing the atrium pressure, mock circulatory system, temperature controller (40 °C), ultrasonic flowmeter (T206, Transonic Systems Inc., Ithaca, New York, U.S.A) for flow monitoring, polygraph (CG-5591, Fukuda Denshi, Tokyo, Japan) for the hemodynamic signal amplification and display, an analog to digital (A/D) data acquisition system (Wavebook/512, U.S.A.) for the data recording, and the external PC (IBM-type desktop personal computer) for the external controller. We used Bjork-Shiley mechanical valves for the left ventricle and Medtronics hall mechanical valves for the right one. And we adopted a newly designed pump – left and right ventricles have large amounts of oil between the inner sac and the outer one. The cannulae were Tigon tubes of 1/2” diameter.

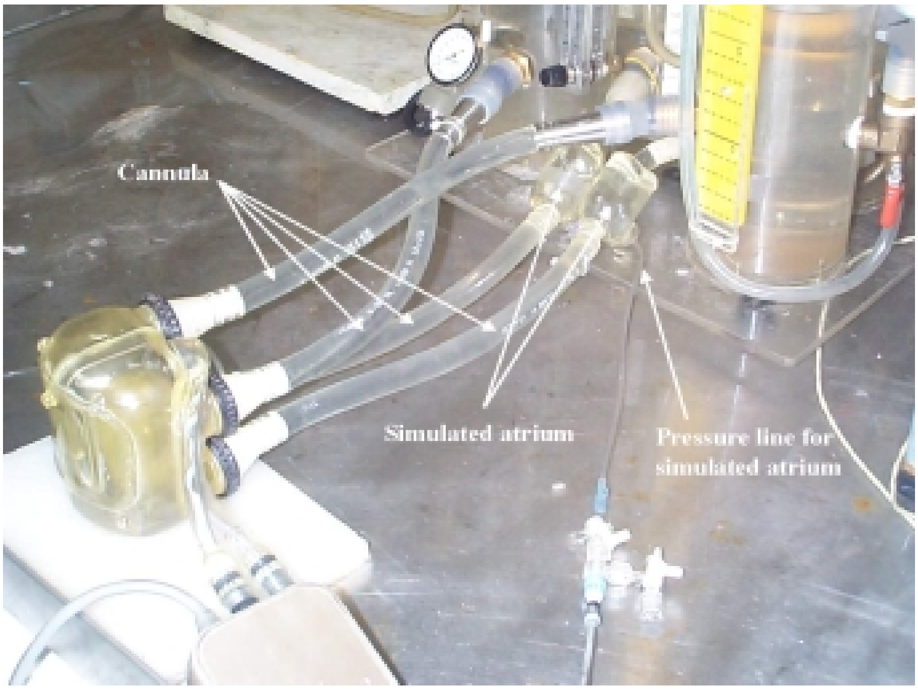

Fig. 3. 7. *In vitro* test equipments for biventricular assist control.

3. 3. 1. *In vitro* experiments of fixed *SV* control

The constants for the ***PO*** and ***AoP*** estimators were heuristically modified (**Table 3. 3)** from the results of **Section 2. 4. 1**. And the control parameters were set heuristically (**Table 3. 4)**. The most important and sensitive control parameters are left current level (CL_L) and the $PTBC_L$. Of these two, the $PTBC_L$ is more important. If the $PTBC_L$ is very low or high, the controller regards the ventricular inflow state as a bad or good filling, respectively. In these cases, the controller controls the BVAD to produce the corresponding minimum ***PR*** or maximum ***PR***, respectively.

Figure 3. 8 shows that the controller changes the ***PO*** in the range of 2.5-4.5 L/min depending on the ***LAP***. We can see that $PTBC_L$ is inverse proportional to ***LAP***, and the velocity is proportional to ***LAP***. In this test, we gave four low atrium pressure and the corresponding $PTBC_L$ reflected this change and the controller adjusted the right velocity, ***PR***, and ***PO*** depending the ***LAP***. Especially, after approximately 300 seconds, very high negative ***LAP*** was simulated, and the MA-BVAD responded to run with the minimum ***PR,*** and the ***LAP*** of – 2 mmHg was monitored. We can adjust this severe case of negative ***LAP***'s response by adjusting the minimum ***PR***, and if we decrease this minimum ***PR***, we can increase from – 2 mmHg.

Table 3. 3. Constants for estimators

Constants	Values
c_0	0.000800
c_1	0.500
c_2	0.001
a_0	0.2797
s	1.494
c	0.00670
v	0.0000024841
a_1	0.00000028545
$mIVP$	-20.0

Table 3. 4. Parameters for fixed ***SV*** control.

Constants	Values
SA_L	57
SA_R	55
Vel_L	30
BT_L	0
BT_R	0
Action cycle	3
CL_L	15
Target $PTBC_L$	23
Step number for the running mean filter	15
Minimum ***PR***	75
Maximum ***PR***	100
Minimum damping level of Vel_R	20
Maximum damping level of Vel_R	70

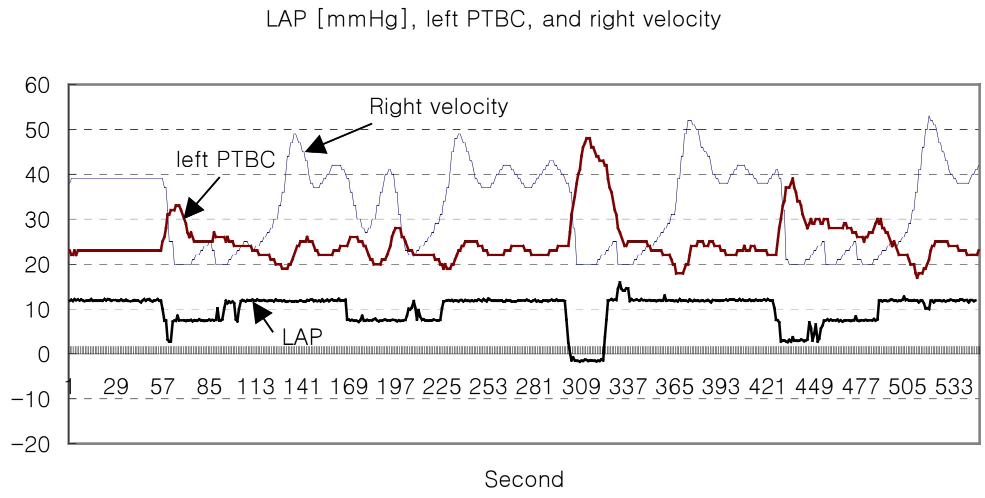

(a)

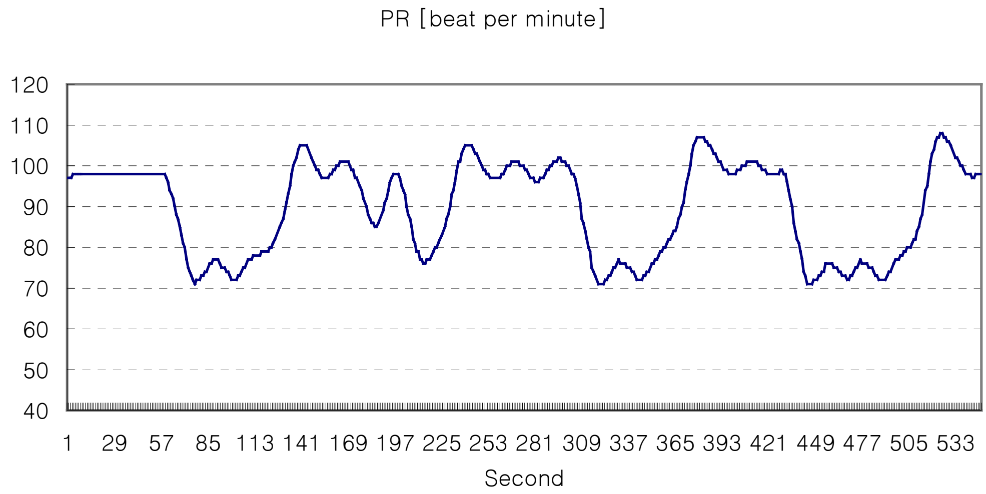

(b)

Fig. 3. 8. *In vitro* test of the fixed ***SV*** control. (a) mean ***LAP***, ***PCT_L***, and right velocity, (b) ***PR***

3. 3. 2. *In vivo* experiments of fixed *SV* control

On the morning of September 30th, the *in vivo* test was performed. **Table 3. 5** and **3. 6** are the constants and parameters for estimators and control. The fixed ***SV*** control algorithm was implemented in an external IBM-compatible desktop PC. We tried to measure the ***PO*** by ultrosonic flowmeter (Transonic Systems Inc., U.S.A.), but failed. Only the ***AoP*** and ***PAP*** can be measured. Thoughout the alive times after surgical operation, the ***AoP*** and ***PAP*** maintained about 80-100 mmHg and 10-20mmHg, respectively. SA_L and SA_R were set 57 and 57. **Figure 3. 9** are the results. From this *in vivo* test, we found there are great gaps between *in vitro* and *in vivo* situations. Therefore, modification of model's constants was required. Heuristically modified constants produced satisfactory results. First difference was the low ***PTBC***. We inferred this phenomenon from the native heart pumping and the reduced atrium's blood volume contrary to that of the *in vitro* test. So target ***PTBC*** was changed to correctly play as a control parameter. Second difference was the ***AoP*** estimator's operational region. We inferred this phenomenon from the native heart pumping and the measuring position of ***AoP***. Finally, mean ***IVP*** is from – 45 to - 50 mmHg for the *in vivo* case, but the *in vitro* test produced from – 20 to -25 mmHg. The fixed ***SV*** control kept the $PTBC_L$ constant by adjusting the ***PR***. **Figure 3. 10** is the view of the monitoring panel during the animal experiment. **Figure 3. 11** are the pictures of putting of 'Yang Jang Gun (we named this sheep like this)' to grass for about one hour.

Table 3. 5. Constants for estimators

Constants	Values
c_0	0.000750
c_1	0.500
c_2	0.001
a_0	0.300
s	1.100
c	0.00670
v	0.0000024841
a_1	0.00000028545
mIVP	-40.0

Table 3. 6. Parameters for fixed ***SV*** control

Constants	Values
SA_L	57
SA_R	57
Vel_L	30
BT_L	0
BT_R	0
Action cycle	3
CL_L	20
Target $PTBC_L$	48
Step number for the running mean filter	20
Minimum ***PR***	75
Maximum ***PR***	100
Minimum damping level of Vel_R	20
Maximum damping level of Vel_R	70

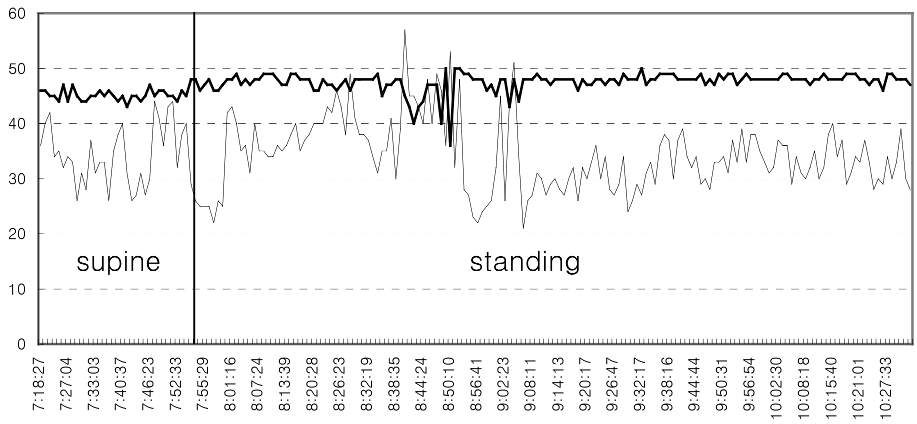

(a)

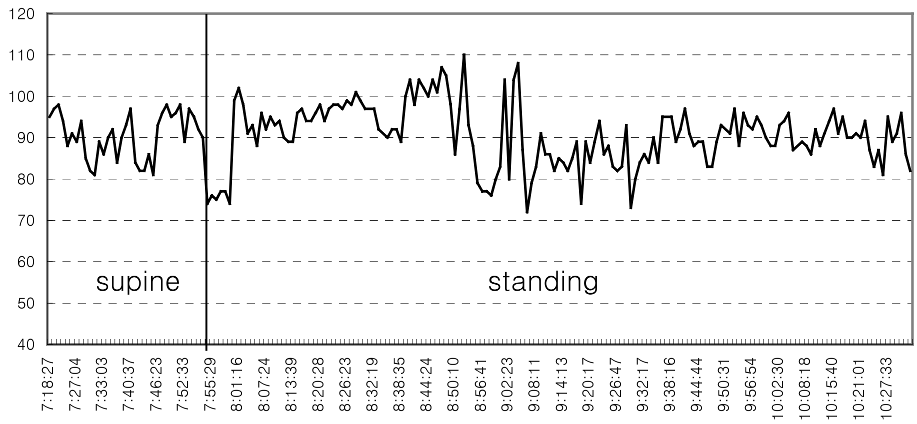

(b)

Fig. 3. 9. Fixed ***SV*** control and hemodynamic parameters during *in vivo* test.

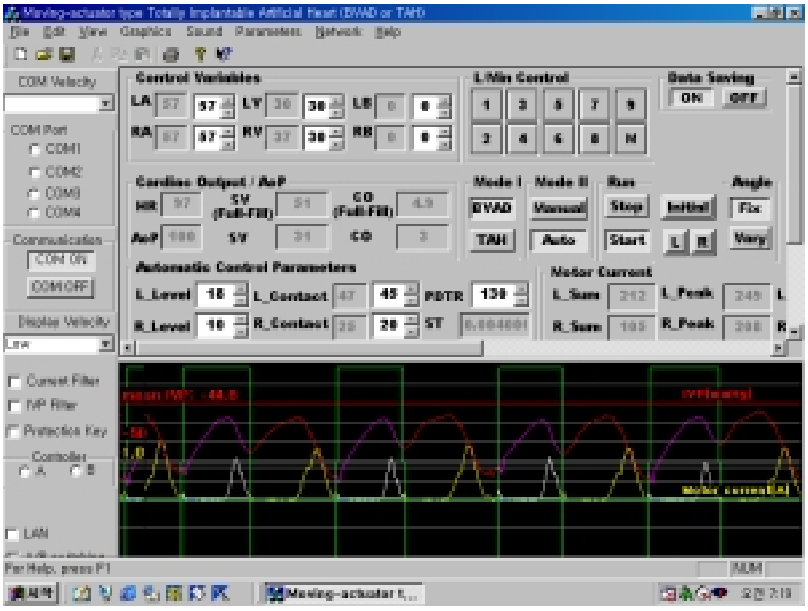

(a)

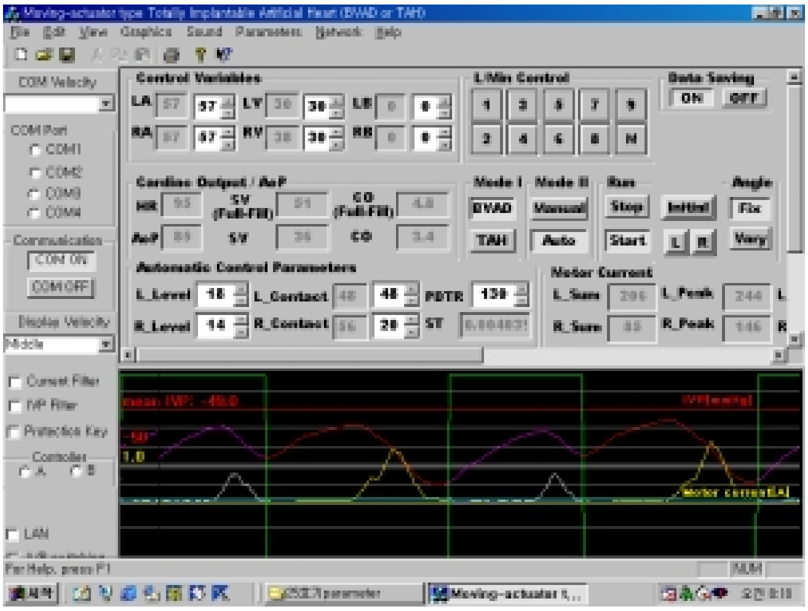

(b)

Fig. 3. 10. Monitoring panel during *in vivo* test.

(a)

(b)

(c)

Fig. 3. 11. Putting to grass for about one hour (11:40 am – 12:40 pm, 20th October). (a) the movement of the 'Yang Jang Gun' by cart, (b) and (c) picture of standing and grazing on the grass field.

3. 3. 3. *In vitro* experiments of fixed *PR* control and *HR*-based control

Figure 3. 12 is the result of the *in vitro* test of fixed ***PR*** control and ***HR***-based control. The linear equation between ***PR*** and ***HR*** was ***PR*** = 2/3***HR*** + 20. The minimum ***PR*** and the maximum ***PR*** were set 60 and 100, respectively. ***PDTR*** was set 100. As we can see, ***PR*** was proportional to ***HR*** and the operational range is between the minimum ***PR*** and maximum ***PR*** even if the ***HR*** is very low (50) or very high (140). We can see that there is very little difference between the target ***PR*** and the real ***PR***. And the delayed response, caused by running mean filtering of 15 beats, cannot be eliminated.

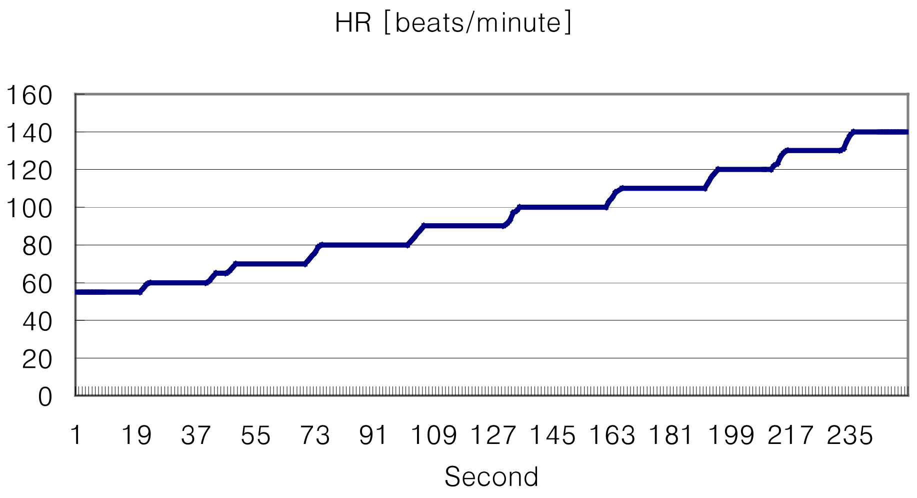

(a)

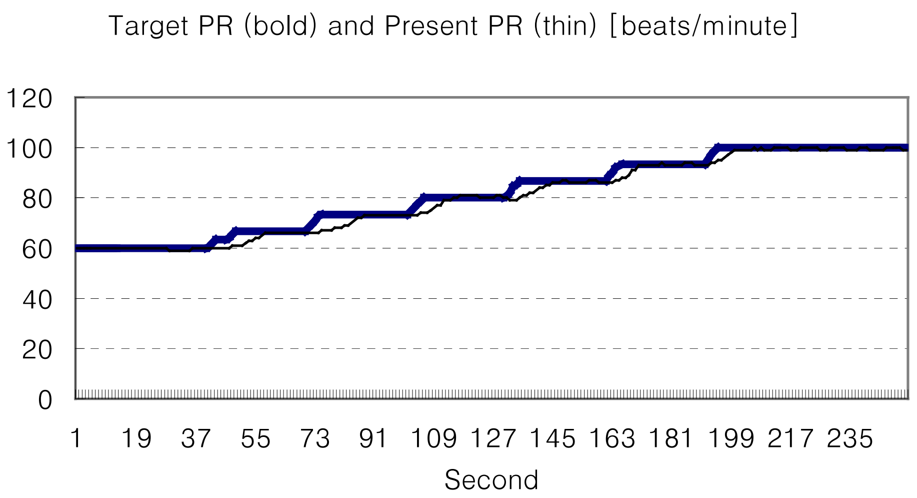

(b)

Fig. 3. 12. *In vitro* performance of fixed ***PR*** control and ***HR*** (native heart rate)-based control. ***PR*** = 2/3***HR***+20, minimum ***PR*** = 60, maximum ***PR*** = 100, (a) ***HR***, (b) target ***PR*** and present ***PR***.

3. 3. 4. *In vitro* experiments of total assist control

The developed preload-sensitive control algorithm was tested in a mock circulatory system (**Figure 3. 13**). Four chamber pressures, equivalent to the ***AoP***, ***PAP***, ***RAP***, and ***LAP*** were measured by a pressure gauge and a water column method. The systemic flow rate was monitored with an ultrasonic flowmeter (T206, Transonic Sytems Inc., Ithaca, New York, U.S.A.). But the mock circulatory system is designed not for biventricular assist configuration but for total artificial heart.

Figure 3. 14 shows the performance of balanced control. We can see high ***LAP*** and high ***RAP*** converged to a stable state within about 30 seconds. All values are uncalibrated. Here we can find that high ***LAP*** (a) converges to a stable state more rapidly than high ***RAP*** (b). We infer this phenomenon from the effect of ***PDTR***. **Figure 3. 15** shows that over a physiological range of preload (2 – 12 mmHg ***RAP***) with simulated bronchial flow rate (approximately 5 % of cardiac output), the ***PO*** responded to the preload change. The sensitivity depends on the required control constants and air volume.

- *Prevention of suction*: Anyone can see this easily *in vitro* test. The recommended experiment protocol is **Table 3. 7.**
- *Balanced output*: This depends on environment heavily, so, careful and reliable *in vitro* environment is important. See **Table 3. 8** and **Figure 3. 14**. We can see in this figure, the extreme unbalanced condition of left and right atrium pressure converged to a stable region in about 30 seconds.
- *Preload sensitive output*: With reliable *in vitro* environment, anyone can verify this by adjusting the pressure of atrium. See **Figure 3. 15**. As the MA-BVAD is active filling device, the sensitive slope is smaller than other known passive filling device. Also, the sensitivity slope depends on the control constants like the other passive-filling devices.

Fig. 3. 13. *In vitro* test equipments for total assist control.

Table. 3. 7. Recommended *in vitro* demonstration of the prevention of suction.

Action	Phenomenon
Step. 1. Right suction	- ***PR*** and ***PO*** decrease - ***RAP*** increase and ***LAP*** decrease
Step. 2. Releasing of suction	- ***PO*** increased and normal ***LAP*** and ***RAP***
Step. 3. Left suction	- ***PR*** and ***PO*** decrease - ***LAP*** increase and ***RAP*** decrease
Step. 4. Releasing of suction	- ***PO*** increased and normal ***LAP*** and ***RAP***

Table. 3. 8. Parameters for total assist control.

Action	Phenomenon
AoP	100 mmHg
PAP	20 mmHg
Valve	Bjork-Shiley mechanical valve
PDTR	115
SA_L	50
SA_R	46
CL_L	20
CL_R	10
$PTBC_L$	21
$PTBC_R$	26
Action cycle of control	3

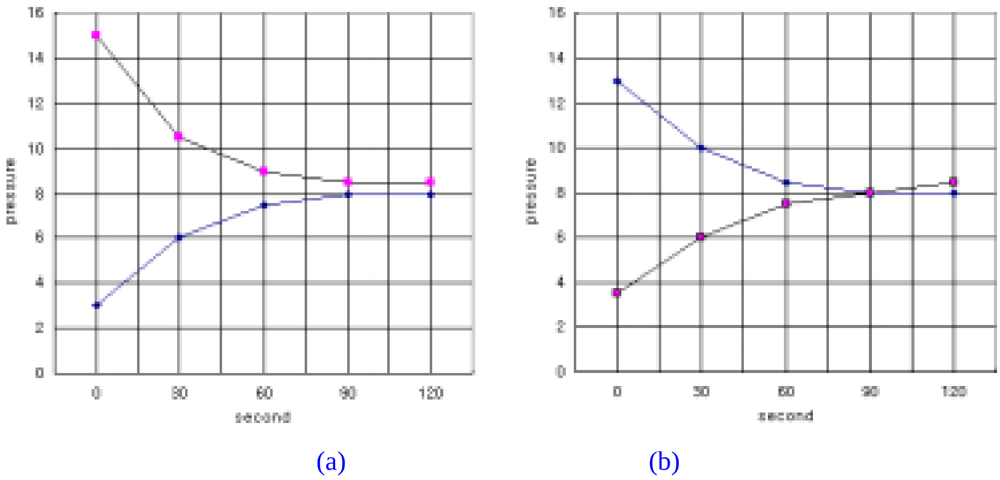

Fig. 3. 14. Performance of balanced output (a) Upper: ***LAP***, lower: ***RAP***, (b) upper: ***RAP***, lower: ***LAP*** [mmHg].

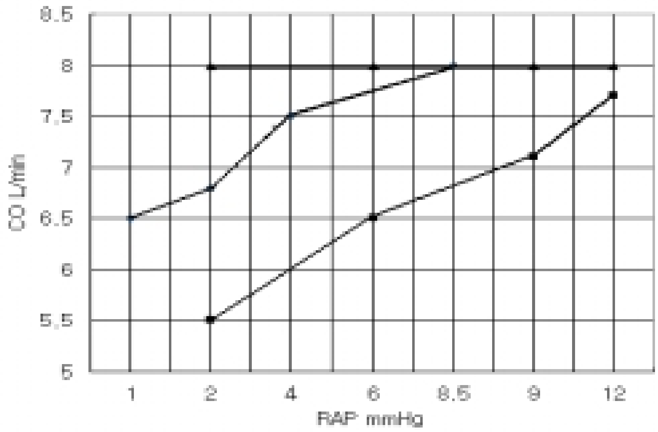

Fig. 3. 15. Total assist control response to preload with various control constants.

3. 3. 5. *In vivo* experiments of total assist control

On April 16th, from 2:00 PM to 3:30 PM, a short *in vivo* test was performed. **Figure 3. 16** is the scene of the *in vivo* test. The inlet and outlet cannulae were not attached to the MA-BVAD. The total assist control performance was testified with the configuration of total artificial heart.

The total assist control algorithm was implemented in portable PC (Ribretto 30, Doshiba, Japan). The hemodynamic measurements were obtained using fluid-filled catheters connected to disposable pressure transducers. At the beginning state, the hemodynamics of the animal was as follows: ***AoP*** was about 70 mmHg and ***RAP*** was very low. So, the hemodynamic state was not good. The animal slept and was supine. During the period of automatic control, the performance of the automatic control had a similar performance of the expert's manual mode control. **Figure 3. 17** is the hemodynamic trend for the manual and automatic control.

The control parameters were like in **Table 3. 9**. All parameters related with motor current are analog to digial converted and uncalibrated. Heuristically found $\boldsymbol{PTBC_L}$ and $\boldsymbol{PTBC_R}$ were 21and 18, respectively. Before the autopsy, various drug test and blood infusion test were performed to increase the ***AoP***. With the effect of high infusion of fluid, the ***LAP*** and ***RAP*** was increased, so the automatic control responded to produce the maximum output ($\boldsymbol{Vel_L}$ = 78, 79, 80), but the ***AoP*** could not be returned to the normal range. It is generally admitted that systemic vascular resistances increase after implantation of TAH in animals, at least during the first post-operative week, before dropping back to preoperative values [47][48][49]. Little has been said about modifications to systemic vascular resistance during TAH assistance. And there are some reports that described progressive loss of *vascular tone* with an *irreversible drop of systemic vascular resistance* [50]. This animal experiment was also concordant with irreversible drop of systemic vascular resistance from undiscovered reasons.

There are reports that an interesting effect of respiration on the atrial pulsation. Since the left and right pumps are operated in the alternate ejection mode, inspiration and expiration result in a 180 out-of-phase effect. There is a delay of approximately 3-5 beats between the right and left ventricles.

Thus, the feedback regulation of the motor speed should be based on the average pump performance of the 5 previous beats or more [43]. **Figure 3. 18** is the control parameters variations. The automatic control produced somewhat high variation of velocity even if the range did not diverse. This variation stemmed from the prescribed respiration effect and the **Figure 3. 19** supports this.

Table 3. 9. Parameters used for *in vivo* test.

Control parameters	Value
PDTR	120
$\boldsymbol{SA_L}$	50
$\boldsymbol{SA_R}$	46
$\boldsymbol{CL_L}$	20
$\boldsymbol{CL_R}$	10
Minimum $\boldsymbol{Vel_L}$	50
$\boldsymbol{PTBC_L}$	18-21 (dominant region: 19, 20)
$\boldsymbol{PTBC_R}$	15-20 (dominant region: 18, 19)

Fig. 3. 16. *In vivo* test of the total assist control of MA-BVAD.

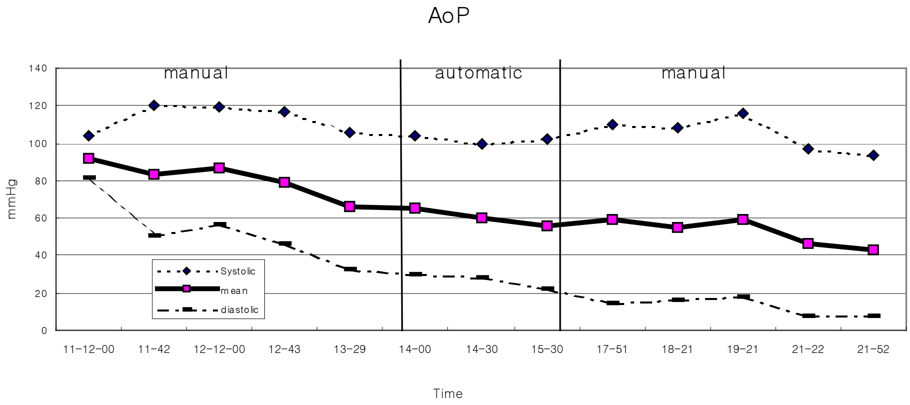
AoP
manual
automatic
manual
mmHg
140
120
100
80
60
40
20
0
Systolic
mean
diastolic
11-12-00
11-42
12-12-00
12-43
13-29
14-00
14-30
15-30
17-51
18-21
19-21
21-22
21-52
Time

(a)

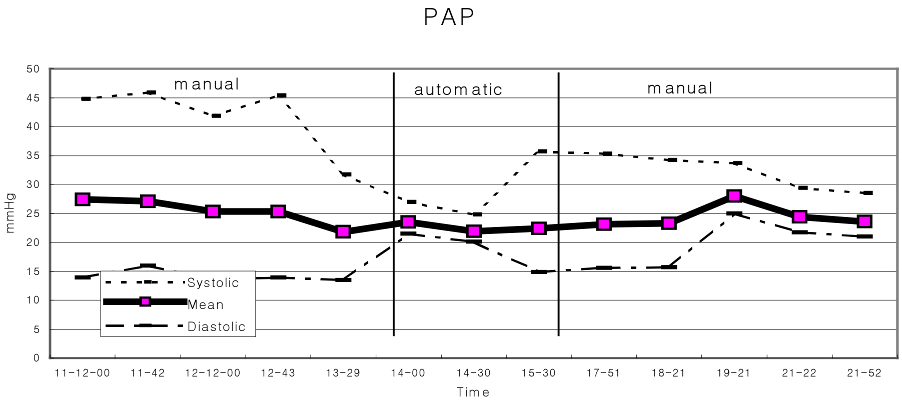
PAP
manual
automatic
manual
mmHg
50
45
40
35
30
25
20
15
10
5
0
Systolic
Mean
Diastolic
11-12-00
11-42
12-12-00
12-43
13-29
14-00
14-30
15-30
17-51
18-21
19-21
21-22
21-52
Time

(b)

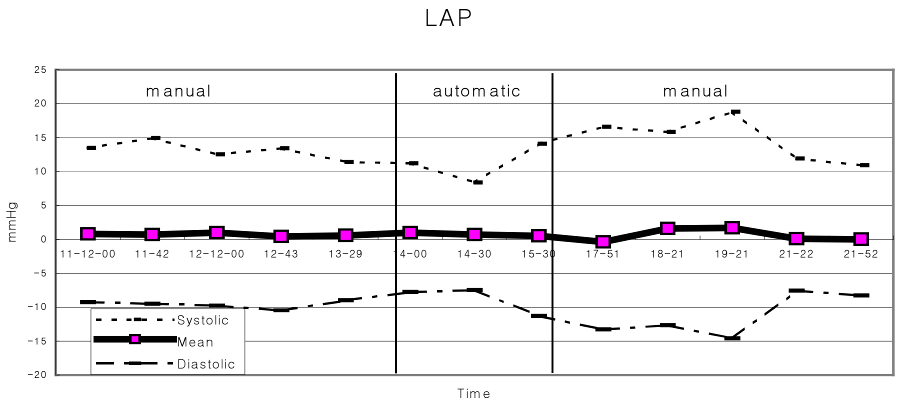
LAP
manual
automatic
manual
mmHg
25
20
15
10
5
0
-5
-10
-15
-20
11-12-00
11-42
12-12-00
12-43
13-29
14-00
14-30
15-30
17-51
18-21
19-21
21-22
21-52
Systolic
Mean
Diastolic
Time

(c)

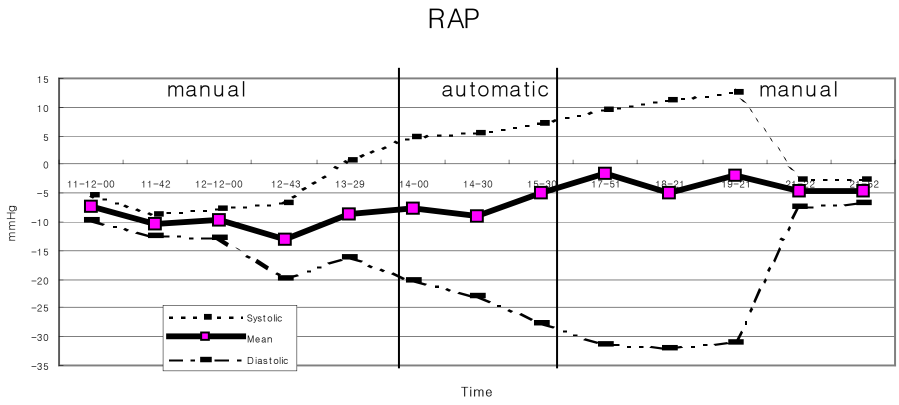

(d)

Fig. 3. 17. Hemodynamic trend. (a) ***AoP***, (b) ***PAP***, (c) ***LAP***, (d) ***RAP***.

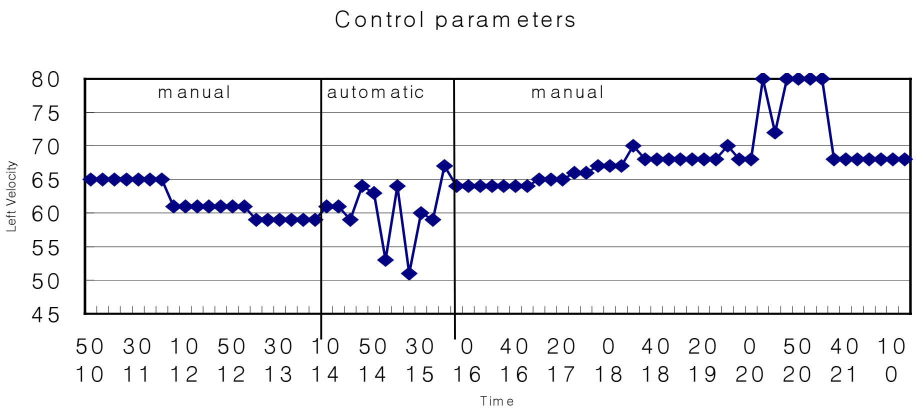

Fig. 3. 18. Variation trend of $\boldsymbol{Vel_L}$.

Fig. 3. 19. The influence of respiration to the other signals.

4. DISCUSSION

4. 1. *PTBC* as a New Preload-Sensitive Parameter and CWM filtering

In this dissertation, motor current was used as a noninvasive signal. Possible noninvasive signals for MA-BVAD are motor currnet and ***IVP***. The comparisons between motor current and ***IVP*** are summarized in **Table 4. 1**. Here, the external disturbances are: position of the MA-BVAD, temperature, pressure sensor's reference, etc. The motor current signal is a stable and noninvasive signal, but it has been known that motor current-based preload information and preload-sensitive control is hard for the volumetrically-coupled active filling TAH device, contrary to the passive filling one. This comes from the fact that the motor current has two informations of preload and afterload for an active filling device. But for the passive-filling device, the ***CL*** is not sensitive, so, high or low ***CL*** does not matter. Proposed ***PTBC*** with proposed ***CL*** overcomes this problem. Because of the circular form of blood ventricle of MA-BVAD, one minor shortcoming of delayed increase of motor current is possible for the case of low velocity. Even if the proposed ***PTBC*** reflects the information of EDV, the preload-sensitivity is lower than that of the passive-filling device. ***PTBC*** only reflects the EDV information. If the higher preload-sensitivity is needed, interventricular volume compensation must in increased.

Table 4. 1. Comparisons between motor current and ***IVP***.

	Motor current	***IVP***
Sensor	Resistance with amplifier	Pressure sensor with amplifier
Information	Afterload information, EDV	Dynamic inflow state of blood sac
Robustness	Robust to external disturbances	Sensitive to external disturbances

As the impulsive noise components will prevent the correct ***PTBC*** and ***mAoP*** estimation, nonlinear CWM filtering is carried out as a preprocessing stage. This filter was verified to have a good capability to cope with nonlinear noise suppression such as the impulsive noise occurred in the motor current or the ***IVP*** signals. Mean-class filtering was verified not to be appropriate for the motor current signals. Experimental results showed that CWM filter with side-length two and central weight one is the most appropriate for not only motor current but also ***IVP*** signals. Further research must be concentrated on the following:

- Consideration of an efficient method to find the contact point between actuator and blood sac by starting in the middle of the current data. This enables us to eliminate the false determination of low ***PTBC*** caused by Gaussian-type noise.

4. 2. Development of Beat-to-Beat Mean *PO* and *AoP* Estimators

The geometric ***SV*** model was studied and the practical implementation lead this study to the development of simplified geometric ***SV*** model. The simplicity of the developed model enables us to use the well-known *pseudoinverse* to determine the constants of the model from real data.

$$PO = SV_L \times PR$$

$$SV_L = SV_{L0} \times f_d(\textit{filling}\ \text{state}) \times f_s(mAoP)$$

$$SV_{L0} = c_0\left(SA_L^2 - SA_R^2\right) + c_1\left(SA_L + SA_R\right)$$

$$f_d(\textit{filling state}) = 1 - \frac{PTBC\left(c_1 - c_0 SA_R + \dfrac{PTBC}{200} c_0\left(SA_L + SA_R\right)\right)}{100\left(c_1 + \dfrac{1}{2} c_0\left(SA_L - SA_R\right)\right)}$$

$$f_s(mAoP) = 1 - c_2\, mAoP$$

If the unexpected and undesirable condition, such as the vessel's chokes from thrombosis or air leakage, do not happened, because the ***PO*** is the outflow of the output port, there is a little possibility between the real and estimated value. Penn State University team utilized the *motor voltage* and *force equilibrium* method for finding the ***AoP***. The developed ***mAoP*** estimation for MA-BVAD is based on the *motor current* and *energy equilibrium* method.

$$mAoP - mIVP_L \cong \left. \frac{a_0 (\sum_0^T i[t] \cdot ST) - s - c\theta - vw\theta - a_1 w^2}{SV_{L0d}} \right|_{\theta = SA_L + SA_R, w = Vel_L}$$

$$SV_{L0d} = SV_{L0} \times f_d(\mathit{filling\ state})$$

As the developed ***mAoP*** estimator needs the information of ***SV***, setting the correct ***PO*** (or ***SV***) estimator prior to ***mAoP*** estimator is required. The developed models produce beat-to-beat mean estimated value. Possible prerequisite considerations before the construction of ***PO*** and ***AoP*** estimators are:

- The air volume in the interventricular space: This has influence upon ***PO*** and ***AoP*** estimations.
- PI gain: ***PR*** and ***PO*** are influenced by the P (Proportional) and I (Integral) gain in the PI control.
- Correct center position: We can say that the reliable center position is an important factor because of its possibility of affecting other parameters related with ***SA***. So reliable positioning is also important for setting a reliable ***PO*** and ***AoP*** estimations.
- ***IVP*** sensor and MA-BVAD position: This has influence upon the ***IVP*** signal, i.e., whether the material which contacts the sensor's membrane is oil or air.
- Type of valve (e.g., mechanical valve or polymer valve): This has influence upon the

valvular regurgitation.

- ■ Communication speed (In this research, serial communication of 38400 [bps, bits per second] was used): This has influence upon the motor current summation data, but if the Eq (2-41) is used, this can be neglected.
- ■ The reproducibility of MA-BVAD (sac, housing, etc)
- ■ Viscosity of oil: The motor current is influenced by this.
- ■ Temperature: This is related with the air volume and the viscosity of oil.
- ■ Simulated atrium: For an active filling device, the inflow characteristics are influenced heavily on this simulated atrium. Also, the atrial pressure must be measured not by the water height but by the measuring the pressure of simulated atrium.
- ■ Filter for motor current signals: In this research, center weighted median (CWM) filter with side-length two and central weight one was used for noise suppression [23].

Further researched must be concentrated on the followings.

- ■ As the active-filling is the major mechanism of our MA-BVAD, the ***PO*** and the hemodynamic characteristics are influenced heavily by the atrium. We can see that a small sized simulated atrium produces undesirable high *water hammer effect*. This prevents the appropriate flow dynamics. In general, heuristic study of *in vitro* test shows that an increased atrial compliance as possible is good for the active-filling MA-BVAD. So, atrium-related hemodynamics and automatic control is a future good research topic.
- ■ Higher precision of f_d(***filling state***) can be accomplished by using the velocity profile of actuator, because ***PTBC*** have a not fully linear relation with the position.

4. 3. Biventricular Assist Control

Three kinds of biventricular assist control modes were studied in this dissertation

- ■ Fixed ***PR*** control mode
- ■ Fixed ***SV*** control mode
- ■ ***HR***-based control mode

The fixed ***PR*** and the fixed ***SV*** controls are well-known control scheme for VAD. The developed fixed ***PR*** control has very simple structure and was verified to have a good performance by *in vitro* test. The fixed ***SV*** control were accomplished by keeping the ***PTBC***, and verified by *in vitro* and *in vivo* test. The developed fixed ***SV*** control has one minor shortcoming. It's the dependency on ***AoP*** and velocity. A high ***AoP*** moved the contact point to the state of good inflow and vice versa from regurgitation volume change. This high ***AoP*** also can change other possible control parameters, like the ***IVP*** because the ***IVP*** reflects the residual air volume. The velocity also has relations with frictional effect on motor current. These minor shortcomings can be also happened in the other motor current-based preload-sensitive control of passive-filling device. Experimental studies showed that this is not a critical problem, under the not very high ***AoP***, e.g., above 150 [mmHg], and the appropriate ***CL*** can cancel the velocity effect.

Finally, ***HR***-based control is the modified version of synchronous control.

- ■ Required ***PR*** = ***f***(***HR***)
- ■ Asynchronous mode
- ■ Requirement of maximum ***PR*** for the exclusion of suction problem

Further researches must be concentrated on the followings.

- Enhancing the precision of ***PR*** calculation: At present, as the variability of ***PR*** is very high, running mean filtering is needed.

In vivo test of the followings must be exhaustively studied.

- The degree of ventricular pressure and volume work
- Treadmill test
- Adequate linear relation between ***HR*** and ***PR***
- Adequate maximum ***PR***
- Reliable methodology to acquire the ***HR*** information, e.g., ECG or heart sound

4. 4. Total Assist Control for the Preparation of Heart Attack

Even if various control parameters have been studied, almost every research team have the pocus on the Starling-like mechanism (preload-sensitive control) by controlling the left EDV. This control mode is referred LMA mode for alternately ejecting TAH. The LMA mode triggered by the left pump fill can protect the lungs and can also respond to venous return change and therefore is a reliable control method for a one-piece TAH. Relying solely on a Starling-like mechanisms passive intrinsic TAH control may be adequate at rest and with mild to moderate exercise, but it requires alteration of external control parameters during times of severe stress [36]. It is expected that patients will use the telemetry to check the implant status at routine intervals [33].

In order to protect the lungs, an LMA emphasized ejection mechanism was designed based on the ***PTBC***. By keeping the ***PTBC*** constant, preload-sensitive and afterload insensitive ***PO*** response for MA-BVAD was achieved.

Developed preload-sensitive control is characterized by

- Preload sensitive, afterload insensitive, and balanced output control
- Motor current-based noninvasive control
- LMA emphasized LMA+RMA mode control
- Fixed ***SV*** and variable ***PR*** mode control

Proposed strategy for the left/right balanced output uses the following.

- ***PDTR***
- Longer $\boldsymbol{SA_L}$ than $\boldsymbol{SA_R}$
- Greater left ventricular volume than right one.
- Compliance window

In one sentence, we can summarized as follow. "*Control to keep over the minimum flow rate, balanced left and right flow rate, appropriate preload.*" Proposed total assist control algorithm was verified to have good performance by *in vitro* and *in vivo* test. After *in vivo* test, we found mean filter for control parameters is essential because of respiration effect. The most important and sensitive control parameters are $\boldsymbol{CL_L}$ and $\boldsymbol{PTBC_L}$. If the $\boldsymbol{PTBC_L}$ is very low or high, the controller regards the ventricular inflow state as a good filling state or a bad one, respectively, and the controller maybe controls the MA-BVAD as the corresponding maximum ***PR*** or minimum ***PR***, respectively.

Even if there are differences between *in vivo* and *in vitro* environment, the pump runs with a maximal and balanced output excluding suction (full-fill and full-output). Even if there are a lot of motor current-based preload-sensitive controls of MA-BVAD [51][52][53][54], the basic characteristics of these are the afterload-sensitive and only guarantee the prevention of severe atrial suction. Further researched must be concentrated on the followings.

- Development of the system for the determination of heart attack
- *In vitro* and *in vivo* (heart attack) test with the cannulae
- Adjustment of control parameters via telemetry, which may be desirable to accommodate operating extremes in some patients as was reported in the research of Penn State University [33]
- Compensation method of $\boldsymbol{Vel_L}$ not by ± 1 but by other methods such as the difference between $\boldsymbol{PTBC_L}$ and target $\boldsymbol{PTBC_L}$ like the ***SV*** control.

5. CONCLUSIONS

PO control and hemodynamic estimation for MA-BVAD were studied. The distinguished approach of this research is to use motor current. The conventional approach is to use not motor current but ***IVP***. It has been known that motor current is robust to external disturbances compared with ***IVP***, but also it has been known that it is hard to find the EDV information from motor current. In this research, a new preload-sensitive parameter, referred to ***PTBC,*** from motor current was proposed and this parameter was shown to be useful for MA-BVAD.

In this research, a combined control architecture was adopted to effectively regulate the various types of controllers. For the biventricular assist controller, fixed ***SV*** controller, fixed ***PR*** controller, and ***HR***-based controller were developed. As the preparation against heart attack, the total assist controller was developed. The fixed ***SV*** controller and the total assist controller were developed using ***PTBC***. Fixed ***PR*** controller was developed based on a simple rule-base. A new ***HR***-based controller for MA-BVAD was developed by modifying synchronous controller, but this controller needs further verification through the *in vivo* test. Developed control algorithms are theoretically simple and verified by the *in vitro* and the *in vivo* test. As for the biventricular assist control, enhancing the precision of ***PR*** which is calculated in the internal controller, treadmill test, and adequate linear relation between ***HR*** and ***PR*** must be further studied. And for the total assist control, exhaustive *in vitro* and *in vivo* performance test with the cannulae must be carried out.

Finally, beat-to-beat mean ***PO*** and ***AoP*** estimators were developed using ***PTBC*** and motor current. The developed ***PO*** estimator can cope with various situations of variable stroke angle, diastolic and systolic dynamics. The developed ***AoP*** estimator was derived from the energy equilibrium. *In vitro* test showed that developed estimators have reliability even though their simplicity. For the noise suppression in the motor current signal, CWM filter was found to have a good performance. Experimental results showed that CWM filter with side-length two and central weight one is the most appropriate choice in the perspectives of detail preservation and waveform.

REFERENCES

[1] R. A. Ott, D. E. Gutfinger, A. B. Gazzaniga, *Cardiac surgery: State of the Art Reviews*, Philodelphia: Hanley & Belfus, Inc., vol. 7, no. 2, p. 461, 1993.

[2] H. C. Kim, *A study on the control of motor-driven artificiai heart*, Ph. D. Dissertation, Dept. of Biomedical Engineering, Seoul National University, Seoul, Korea, 1989.

[3] B. G. Min, H. C. Kim, S. H. Lee, J. W. Kim, J. T. Kim, I. Y. Kim, S. W. Kim, P. D. Diegel, and D. B. Olsen, "A moving-actuator type electromechanical total artificial heart-part I: linear type and mock circulation experiments," *IEEE Trans. Biomedical Engineering*, vol. 37, no. 12, pp. 1186-1194, Dec. 1990.

[4] B. G. Min, H. C. Kim, J. W. Choi, G. H. Ryu, K. P. Seo, J. R. Rho, H. Ahn, S. W. Kim, P. D. Diegel, and D. B. Olsen, "A moving-actuator type electromechanical total artificial heart-part II: Circular type and animal experiment," *IEEE Trans. Biomedical Engineering*, vol. 37, no. 12, pp. 1195-1200, Dec. 1990.

[5] B. G. Min, S. J. Kim, M. J. Choi, W. W. Choi, and S. K. Park, "Modeling technique for development of the moving-actuator total artificial heart," *Waseda International Congress of Modeling and Simulation Technology for Artificial Organs*, p. 5, Appendix 1, 2, 1996.

[6] S. K. Park, M. J. Choi, S. J. Kim, and B. G. Min, "The compliance model of the inter-ventricular space in the moving-actuator type total artificial heart," *Waseda International Congress of Modeling and Simulation Technology for Artificial Organs*, p. 74, Appendix 3, 4, 1996.

[7] M. Urino and M. Innocenti, “Modeling arterial hypotension during hemodialysis,” *Artificial Organs*, vol. 21, no. 8, pp. 873-890, 1997.

[8] K. S. Om and B. G. Min, "Relation between multidimensional linear interpolation and fuzzy reasong," *J. Korea Fuzzy Logic and Intelligent Systems*, vol. 6, no. 4, pp. 34-38, 1996.

[9] K. S. Om and B. G. Min, "Relation between multidimensional linear interpolation and regularization networks," *J. Korea Fuzzy Logic and Intelligent Systems*, vol. 7, no. 3, pp. 89-95, 1997.

[10] K. S. Om, W. W. Choi, J. M. Ahn, S. K. Park, Y. H. Jo, J. S. Choi, J. J. Lee, H. C. Kim, and B. G. Min, "Experimental approach for the estimation of cardiac output of left ventricular assist device using multi-dimensional interpolation technique," *KOSOMBE Spring Conference*, pp. 232-234, 1996.

[11] D. E. Goldberg. *Genetic algorithm in search, optimization, and machine learning*, Reading, Massachusetts: Addison-Wesley, 1989.

[12] H. J. Nabel, K. P. Schmitz, W. Urbaszek, W. Scharf, K. Emmrich, and H. Klinkmann, "Relationship between design and control of artificial heart for protection of the right/left balance," *Int. J. Artificial Organs*, vol. 13, no 1, pp. 51-54, 1990.

[13] T. Tanaka, S. Takatani, M. Umezu, T. Nakatani, S. Adachi, H. Noda, S. Fukuda, H. Takano, and T. Akutsu,, “Factors effecting left-right heart output differences in artificial heart implanted animal,” *Trans. Am. Soc. Artif. Intern. Organs*, 1985.

[14] S. H. Lee, *A study on the control of Korean total artificial heart and transcutaneous energy transmission method*, Ph. D. Dissertation, Dept. of Biomedical Engineering, Seoul National University, Seoul, Korea, 1992.

[15] I. Y. Kim, *Analysis of a totally implantable electromechanical artificial heart using computer simulation*, Ph. D dissertation, Dept. of Biomedical Engineering, Seoul national university, Seoul Korea, 1993.

[16] A. J. Snyder, G. Rosenberg, and W. S. Pierce, “Noninvasive control of cardiac output for alternately ejecting dual-pusherplate pumps,” *Artificial Organs*, vol. 16, no. 2, pp. 189-194, 1992.

[17] B. C. Kuo, *Automatic control systems*, Upper Saddle River: Prentice-Hall, 1992.

[18] S. Haykin, *Adaptive Filter Theory*, Upper Saddle River: Prentice-Hall, 1996.

[19] K. S. Om, J. M. Ahn, and B. G. Min, "Static state hemodynamic variables estimation model for the moving-actuator type total artificial heart. Part. I - cardiac output estimation, " *Int. J. Artificial Organs*, vol. 22, no. 1, pp. 21-26, 1999.

[20] K. S. Om, Y. H. Jo, and B. G. Min, "Static state hemodynamic variables estimation model for the moving-actuator type total artificial heart. Part. II – aortic pressure estimation, " *Int. J. Artificial Organs*, vol. 22, no. 2, pp. 108-112, 1999.

[21] C. Toumazou , Circuits & Systems Tutorials, *IEEE Intern. Symp. Circuits & Systems*, 1994.

[22] K. S. Om, *A Study on the development of digital subtraction angiographic image processing system*, M.S. Dissertation. Department of Electronics Engineering, Inha University, Inchon, Korea, 1996.

[23] S. J. Ko and Y. H. Lee, "Center weighted median filters and their applications to image enhancement," *IEEE Trans. Circuits and Syst.*, vol. CAS-38, no. 9, Sept. 1991.

[24] I. Pitas, *Digital Image Processing Algorithms*, Upper Saddle River: Prentice-Hall, 1993.

[25] E. Ataman, V. K. Aatre, and K. M. Wong, "A fast method for real-time Median filtering," *IEEE Trans. Acoust., Speech, signal Processing*, vol. ASSP-28, pp. 415-421, Aug. 1980.

[26] I. Pitas, "Fast algorithms for running ordering and Max/Min calculation," *IEEE Trans. Circuits and Syst*. vol. CAS-36, no. 6, pp. 795-804, June, 1989.

[27] T. S. Huang, G. J. Yang, G. Y. Tang, "A fast two-dimensional median filtering algorithm," *IEEE Trans. Acoust., Speech, Signal Processing,* vol. ASSP-27, no. 1, pp. 13-18, Feb. 1979.

[28] 성호경, 김기환, *생리학*, 서울: 의학문화사, 1997.

[29] A. J. Snyder, G. Rosenberg, and W. S. Pierce, "Noninvasive control of cardiac output for alternately ejecting dual-pusherplate pumps," *Artificial Organs*, vol. 16, no. 2, pp. 189-194, 1992.

[30] J. J. Carr and J. M. Brown, *Introduction to Biomedical Equipment Technology*, Englewood Cliffs, New Jersey: Prentice-Hall, inc., p. 14, 1993.

[31] F. H. Netter, *The CIBA Collection of Medical Illustration*, vol. 5-Heart, Summit, New Jersey: CIBA, 1978.

[32] V. C. Rideout, *Mathematical and computer modeling of physiological systems*, Englewood Cliffs, New Jersey: Prentice-Hall, Inc. pp. 109-110, 1991.

[33] W. J. Weiss, G. Rosenberg, A. J. Snyder, W. S. Pierce, W. E. Pae, H. Kuroda, M. A. Rawhouser, G. Felder, J. D. Reibson, T. J. Cleary, S. K. Ford, J. A. Marlotte, R. A. Nazarian, and D. L. Hickst, "Steady state hemodynamic and energetic characterization of the Penn State/3M health care total artificial heart," *Trans. Am. Soc. Artif. Intern. Organs*, vol. 45, no. 3, pp. 189-193, 1999.

[34] A. Andrade, D. Nicolosi, J. Lucchi, J. Biscegli, A. C. F. Arruda, Y. Ohashi, J. Mueller, E. Tahama, J. Glueck, and Y. Nose, "Auxiliary total artificial heart: a compact electromechanical artificial heart working simultaneously with the natural heart," *Artificial Organs*, vol. 23, no. 9, pp. 876-880, 1999.

[35] M. Ishikawa, G. B. Jacobs, N. Uchida, M. Nasu, T. Oku, H. Emoto, T. Watanabe, W. A. Smith, R. J. Kiraly, H. Harasaki, and Y. Nose, "Mode comparison study for a completely implantable TAH (CITAH) system," *Trans. Am. Soc. Artif. Intern. Organs*, vol. 35, pp. 194-200, 1987.

[36] G. S. Allen, K. D. Murray, and D. B. Olsen, "Control of the artificial heart," *Trans. Am. Soc. Artif. Intern. Organs*, pp. 932-937, 1996.

[37] T. Yambe, S. Nitta, Y. Katahira, K. Izumi, and H. Taketa, "Estimation of the following cardiac output using sympathetic tone and hemodynamics for the control of a total artificial heart," *Int. J. Artificial Organs*, vol. 15, no. 6, pp. 606-610, 1992.

[38] K. Taguchi, T. Hijikata, T. Mochizuke, M. Matsumura, and T. Hasegawa, "Elimination of monitoring problems by permanent signalization of aortic nerve activity for control of artificial heart," *Trans. Am. Soc. Artif. Intern. Organs*, vol. 27, pp. 123-126, 1981.

[39] B. G. Min, I. Y. Kim, and H. C. Kim, "Different stroke volumes for the left and right ventricles in the moving-actuator type total artificial heart," *Int. J. Artificial Organs*, vol. 16, pp. 45-50, 1993.

[40] D. B. Olsen, R. K. White, J. W. Long, and P. S. Kahnwilkar, “Right-left ventricular output balance in the totally implantable artificial heart,” *Int. J. Artificial Organs*, vol. 14, no. 6, pp. 359-64, 1991.

[41] S. Takatani, H. Harasaki, S. Koike, I. Yada, R. Yozu, L. Fujimoto, S. Murabayashi, G. Jacobs, R. Kiraly, and Y. Nose, “Optimum control mode for a total artificial heart,” *Trans. Am. Soc. Artif. Intern. Organs*, vol. 28, pp. 148-153, 1982.

[42] M Ishikawa, G. B. Jacobs, N. Uchida, M. Nasu, T. Oku, H. Emoto, T. Watanabe, W. A. Smith, R. J. Kiraly, H. Harasaki, and Y. Nose, “Mode comparison study for a completely implantable TAH (CITAH) system”, *Trans. Am. Soc. Artif. Intern. Organs*, vol. 33, pp. 194-200, 1987.

[43] S. Takatani, M. Shiono, T. Sasaki, I. Sakuma, G. P. Noon, Y. Nose, and M. E. DeBakey, “Left and right pump output control in one-piece electromechanical total artificial heart,” *Artificial Organs*, vol. 17, no. 3, pp. 176-184, 1993.

[44] K. Imach, T. Chinzei, K. Maeda, K. Mabuchi, Y. Abe, T. Yonezawa, M. Asano, M. Suzukawa, A. Kouno, T. Ono, and I. Fujimasa, “Predictive control of total artificial heart during exercise,” In: Vasku J. ed. Total artificial heart-problems of regulation (Proc. ISAO-ESAO satellite symposium). Brno: University J. E. Purkyne, pp. 101-110, 1988.

[45] K. S. Om, J. M. Ahn, C. Y. Park, G. J. Yun, H. S. Cho, J. W. Kim, Y. H. Jo, W. E. Kim, Y. N. Park, J. S. Choi, J. W. Park, S. W. Choi, W. G. Kim, and B. G. Min, “The automatic control of the moving-actuator type totally-implantable artificial heart using the motor current,” *APCMBE Conference*, vol. 4, 1999.

[46] Y. H. Lee and A. T. Fam, "An edge gradient enhancing adaptive order statistic filter," *IEEE Trans. Acoust., Speech, Signal Processing*, vol. ASSP-35, no. 5, pp. 680-695, May, 1987.

[47] T. H. Stanley, W. S. Liu, and S. Gentry, “Blood and urine catecholamine concentrations after implantation of artificial heart,” *J. Thorac. Cardiovasc. Surg.*, vol. 17, pp. 704-10, 1976.

[48] T. Murakami, K. Ozawa, H. Harasaki, G. Jacobs, R. Kiraly, Y. Nose, “Transient and permanent problems associated with the total artificial heart implantation,” *Trans. Am. Soc. Artif. Intern. Organs*, vol. 25, pp. 239-247, 1979.

[49] K. Imachi, I. Fujimasa, M. Nakajima, K. Mabuchi, S. Tsukagoshi, K. Motomura, A. Miyamoto, N. Takido, N. Inou, and A. Kouno, T. Ono, and K. Atsumi, “Overall analysis of the causes of pathophysiological problems in total artificial heart in animals by cardiac rereptor hypothesis,” *Trans. Am. Soc. Artif. Intern. Organs*, vol. 30, pp. 591-596, 1984.

[50] P. Deleuze, D. Y. Loisance, N. Shiiya, F. Wan, M. L. Hillion, C. Benvenuti, Y. Heurtematte, and J. P. Cachera, “Irreversible drop of systemic vascular resistances in patients implanted with a Jarvik total artificial heart,” *Int. J. Artificial Organs*, vol. 14, no. 5, pp. 286-289, 1991.

[51] H. C. Kim and B. G. Min, “In vitro development of automatic control for the moving-actuator type total artificial heart (TAH),” *Heart Replacement-Artificial Heart 4*, Tokyo: Springer-Verlag, pp. 361-365. 1993.

[52] M. H. Lee, J. M. Ahn, B. G. Min, S. Y. Lee, and C. H. Park, “Total artificial heart using neural and fuzzy controller,” *Artificial Organs*, vol. 20, no. 11, pp. 1220-1226, 1999.

[53] B. G. Min, J. M. Ahn, W. G. Kim, and J. R. Roh, "Automatic control algorithm for cardiac output regulation of the total artificial heart (TAH)," *Heart Replacement-Artificial Heart 5*, Tokyo: Springer-Verlag, pp. 293-296. 1996.

[54] W. W. Choi, H. C. Kim, and B. G. Min, "A new automatic cardiac output control algorithm for moving actuator total artificial heart by motor current waveform analysis," *Int. J. Artificial Organs*, vol. 19, no. 3, pp. 189-196, 1996.

[55] M. T. Swartz, H. S. Borovetz, P. J. Miller, H. E. Mitchell, J. T. Watson, B. P. Griffith, D. G. Pennington, and P. M. Portner, "Evaluation of an implantable ventricular assist system for humans with chronic refractory heart failure: technical considerations," *Trans. Am. Soc. Artif. Intern. Organs*, vol. 41, pp. 27-31, 1995.

[56] J. T. Watson, "Prospects for implantable circulatory support," *Heart Replacement-Artificial Heart 5*, Tokyo: Springer-Verlag, pp. 3-7. 1996.

[57] F. D. Altieri and J. T. Watson, "Implantable ventricular assist systems," *Artificial Organs*, vol. 11, no. 3, pp. 237-245, 1987.

국문 초록

인공 심장 연구의 연구 추세는 이식형 시스템(implantable system)으로 바뀌고 있으며, 이식형 심실 보조 장치(ventricular assist device, VAD)의 역할은 여러가지 이유로 인해서 시간의 흐름과 더불어 점점 더 증대되고 있다. 본 논문에서는 이동 작동기형 양심실 보조 장치(moving-actuator type biventricular assist device, MA-BVAD)의 펌프 박출량 제어에 관한 연구가 수행되었다. VAD 의 펌프 박출량 제어 기법으로는 고정 박동수 제어 (fixed pump rate control), 충만-비움 제어(full-to-empty control, pump on full control), 동기 제어(synchronous control)의 세가지가 알려져 있으며, 제대로 작동하고 있는지 외부에서 확인할 수 있는 박출량 정보 및 기타 정보를 제공해야 한다.

본 연구에서는 여러 종류의 제어기를 효과적으로 이용하기 위하여 연합 제어 구조(combined control architecture)를 채택하였다. 양심실 보조 제어로 충만-비움 제어기, 고정 박동수 제어기, 심박동수 기반 제어기(heart rate-based controller)의 3 가지 제어기를 개발하였으며, 심장 발작(heart attack)이 발생할 경우에 대비한 완전 보조 제어기를 개발하였다. 특히, 이 중 충만-비움 제어는 신뢰성과 더불어 혈액의 적절량을 판단하여 보조한다는 점에서 중요 연구 과제로 여겨져 왔다. 충만-비움 제어 알고리듬을 개발하려면 혈액 주머니의 확장기말 용적(end-diastole volume, EDV)을 판별할 수 있는 파라메터가 필요한데, 지금까지는 MA-BVAD 에 관련하여 심실간 공간 압력(interventricular pressure, ***IVP***)이 활용되어져 왔다. ***IVP*** 는 혈류의 동적인 유입 정보에 효과적이나 압력 센서가 외란에 강인하지 못하는 단점이 있다. 반면 모터 전류는 외란에 강인하나 강제 유입 시스템에서는 박출하고자 하는 후부하와 유입되는 전부하의 두 정보를 동시에 반영한다는 점 때문에 전부하 민감 제어에 제대로 활용되지 못했다. 본 연구에서는 MA-BVAD 처럼 능동형 유입 장치를 위한 새로운 전부하 민감 파라메터인 접촉전 비율 시간(percent time before contact, ***PTBC***)을 측정된 모터 전류를 이용하여 계산하는 방법을 제안하였다. ***PTBC*** 는 EDV 에 직접적으로 관련된 좋은 정보이므로 충만-비움 제어와 완전 보조 제어를 구축하는데 사용되었으며, 개발된 충만-비움 제어와 완전 보조 제어는 체외 모의 순환 장치와 체내

실험을 통하여 좋은 성능을 가짐을 확인하였다. 고정 박동수 제어는 간단한 규칙 기반으로 구현하였으며, 새로운 제어 방법의 시도로서 심박동수 기반의 제어 알고리듬을 개발하였는데 변형된 동기 제어 방식으로 볼 수 있겠다. 그러나 제안된 심박동수 기반의 제어는 체내 실험을 통하여 많은 검증이 필요하다.

마지막으로, 박동마다의 평균 펌프 박출량과 평균 대동맥압을 모니터링하기 위하여 ***PTBC*** 와 모터 전류에 기반한 추정자를 개발하였다. 평균 박출량 추정자는 가변 각도, 확장기, 수축기의 동역학 등 다양한 환경을 반영할 수 있다. 개발된 대동맥압 추정자는 에너지 보존에 기반하여 유도되었다. 개발된 추정자들은 물리적 의미를 갖고 있으며, 간단한 모델이나 신뢰성이 있음을 체외 모의 순환 장치 및 체내 실험을 통하여 확인하였다. ***PTBC*** 와 추정자의 정확도를 기하기 위해서 모터 전류 속의 잡음 제거로 중점 가중 메디안 필터가 고려되었으며, 실험 결과에 의하면 측길이가 2 이고 중앙 가중치가 1 인 중점 가중 메디안 필터가 모터 신호의 세밀성과 파형 측면에서 적절했다.

주요어: 펌프 박출량, 대동맥압, 인공 심장 제어, 양심실 보조 장치

학 번: 96431-803

Appendix

: Proof of a CWM Filter Property and C-Program Source of a CWM Filter

Two dimensional signal output $Y(i,j)$ of the CWM filter is given by

$$Y(i,j) = median\{X(i-s, i-t),\ 2K\ \ copies\ \ of\ \ X(i,j) \mid s,t \in W\}.$$

window length = $2L+1$, central weight = $2K+1$

■ ***Property of CWM filter:*** The output $Y(i,j)$ of a CWM filter with window size $2L+1$ and central weight $2K+1$ is represented by

$$Y(i,j) = median\{X_{ij}(L+1-K;2L+1),\ X_{ij}(L+1+K;2L+1),\ X(i,j)\}.$$

where $X_{ij}(r;2L+1)$ is the rth smallest one among $2L+1$ samples within the window centered at (i,j), and $X(i,j)$ is the input value at the center.

Proof:

$L+1$: median for original set (M1)

$L+1+K$: median for extended set (M2)

Case 1:

Suppose $X(i,j) < X_{ij}(L+1\text{-}K;2L+1)$.

Then in the extended set there are $L+1+K$ (M2, from $L+1-K+2K = L+1+K$) values less than or equal to $X_{ij}(L+1\text{-}K;2L+1)$.

So, $X_{ij}(L+1-K;2L+1)$ is the median for the extended set.

And, $X(i,j) < X_{ij}(L+1-K;2L+1) <= X_{ij}(L+1+K;2L+1)$.

Namely, the output $Y(i,j)$ = median $\{X_{ij}(L+1-K;2L+1), X_{ij}(L+1+K;2L+1), X(i,j)\}$.

Case 2:

Suppose $X_{ij}(L+1+K;2L+1) < X(i,j)$

Then in the extended set there are $L+1+K$ (M2) values less than or equal to $X_{ij}(L+1+K;2L+1)$.

So, $X_{ij}(L+1+K;2L+1)$ is the median for the extended set.

And, $X_{ij}(L+1-K;2L+1) <= X_{ij}(L+1+K;2L+1) < X(i,j)$.

Namely, the output $Y(i,j)$ = median $\{X_{ij}(L+1-K;2L+1), X_{ij}(L+1+K;2L+1), X(i,j)\}$.

Case 3:

Suppose $X(i,j) = X_{ij}(L+1-K+m;2L+1)$, $0<=m<=2K$.

Then there are L-K+m values less than or equal to $X_{ij}(L-K+m;2L+1)$.

And, $L-K<=L-K+m<=L+K$.

So, in the extended set the lower bound L-K becomes $(L-K)+(2K+1)=L+\mathrm{K}+1$ (M2),

and, $X(i,j) = X_{ij}(L+1-K+m;2L+1)$ is selected as the output.

And, $X_{ij}(L+1-K;2L+1) <= X(i,j) <= X_{ij}(L+1+K;2L+1)$.

Namely, the output $Y(i,j)$ = median $\{X_{ij}(L+1-K;2L+1), X_{ij}(L+1+K;2L+1), X(i,j)\}$.

The cases of one and three or more dimensions are analogous in every way. Q.E.D.

```
// C program  source of a CWM filter

// buffer for CWM filtering~
int cwm_buff[9][20];
int new_cwm_buff[9][20];

void filtering1(void)
{
        value[0]=CWM_filter(0, 2, 1); // current: value[0]
}

int CWM_filter(int x, int L, int w) //  L: side length,  w: side weight,  total length= (L*2+1)+(w*2)
{
for(i=0;i<=L*2-1;i++)
  {
        cwm_buff[x][i]=cwm_buff[x][i+1];
  }
  cwm_buff[x][L*2]=value[x];

for(i=0;i<=L*2;i++)
  {
        new_cwm_buff[x][i]=cwm_buff[x][i];
  }

  for(i=0;i<=w;i++)         // center weighting~: adding center value~
  {
        new_cwm_buff[x][L*2+i+1]=value[x];
  }

  for(i=0;i<=2*L+2*w-1;i++) // new sorting routine~: bouble sort
  {
        for(j=i+1;j<=2*L+2*w;j++)
       {
          if(new_cwm_buff[x][i]>new_cwm_buff[x][j])
          {
                temp = new_cwm_buff[x][i];
                new_cwm_buff[x][i]=new_cwm_buff[x][j];
                new_cwm_buff[x][j]=temp;
          }
        }
  }
  cwm_buff[x][L] = new_cwm_buff[x][L+1]; // for running filtering~
  return new_cwm_buff[x][L+1];
}
```

Acknowledgement

Heartful thanks must be given to all who gave me the *chance* to study, the *courage* to carry out my study without frustration, and the *support* to complete my Ph. D. program. I, hereby, declare that I will use all my knowledge and powers, that I have acquired through last Ph. D. period, for the prosperities of mankind.

- 孟子
- 第六 告子篇
- 告子章句 下
- 第十五 天將降大任於是人也章

孟子曰,

舜은 發於 견묘之中하고, 溥說은 擧於版책之間하고, 膠력은 擧於魚鹽之中하고 管夷吾는 擧於士하고, 孫叔敖는 擧於海하고, 百里奚는 擧於市하니라. 故로 天將降大任於是人也인댄 必先苦其心志하며 勞其筋骨하며 餓其體膚하며 空乏其身하여 行拂亂其所爲하나니 所以動心忍性하여 曾益其所不能이니라.

人恒過然後에 能改하나니, 困於心하며 衡於慮而後에 作하며, 徵於色하며 發於聲而後에 喩니라. 入則無法家拂士하고, 出則無敵國外患者는 國恒亡이니라. 然後에 知生於憂患而死於安樂也니라.

맹자왈,

순임금은 밭 가운데서 등용되었고, 부열은 성벽 쌓는 사이에서 등용되었으며, 교력은 생선과 소금 파는 데서 등용되었고, 관중은 감옥에서 등용되었으며, 손숙오는 바닷가에서 등용되었고, 백리해는 시장거리에서 등용되었다. 그러므로 하늘이 장차 그들에게 대임을 내리시려면, 반드시 먼저 그들의 마음을 괴롭히고, 그들의 근육과 뼈를 수고스럽게 하며, 그들의 육체를 굶주리게 하고, 그들의 몸을 아무것도 없게 하여, 그들의 행함이 할 바에 어긋나게 하거니와, 이는 바로 그 마음을 움직여서 성질을 참아 그 하지 못하는 바를 할 수 있게 더해 주기 위한 것이다.

사람은 언제나 잘못을 저지른 뒤에라야 능히 고칠 수 있는 법이니, 마음이 괴로와지고 계획이 어긋난 뒤에라야 분발하며, 표정으로 나타내고 말소리를 낸 뒤에라야 깨닫게 된다. 안으로는 법도 있는 세신과 도와주는 현사가 없고, 밖으로는 적국과 외환이 없는 자는 나라가 항상 망한다. 그런 뒤에라야 근심하고 걱정하는 속에서는 살고, 편안하고 즐거운 속에서는 죽는다는 것을 알게 되는 것이다.

Vita

Kyong-Sik Om was born in Seoul, Korea on the 5th of August of the lunar calender, 1971. He graduated from Seon-In High School, Inchon, Korea. He received the B.S. and M.S. degrees in Electronics Engineering from Inha University, Inchon, Korea, in 1994 and 1996, respectively. Since 1996, he has worked as the Ph.D. condidate in Biomedical Engineering at Seoul National University, Seoul, Korea.

Publications

Domestic Conference

1. 엄경식, 정동석, "방향성 정보에 기초한 경계선 검출," *대한전자공학회 하계종합학술대회 논문집*, vol. 17, no. 1, pp. 748-752, 1994.

2. 엄경식, 김진용, 정동석, "경계선 향상을 위한 적응적 비선형 필터의 구현," *신호처리합동학술대회 논문집*, vol. 7, no. 1, pp. 1046-1049, 1994.

3. 엄경식, 문철홍, 정동석, "통합적 경계선 검출," *신호처리합동학술대회 논문집*, vol. 8, no. 1, pp. 393-396, 1995.

4. K. S. Om and J. H. Chung, "Detection of left venricular contours in DSA images," *Korean Signal Processing Conference*, vol. 8, no. 1, pp. 530-533, 1995.

5. 엄경식, 정재호, "DSA 영상처리 시스템의 구현," *신호처리합동학술대회 논문집*, vol. 8, no. 1, pp. 534-538, 1995.

6. 엄경식, 정재호, "DSA 영상에서의 혈관 직경 추적," *신호처리합동학술대회 논문집*, vol. 8, no. 1, pp. 539-542, 1995.

7. 엄경식, 정재호, "R-SAM 예측기와 Huffman 부호화에 기초한 의료영상 무손실 압축," *신호처리합동학술대회 논문집*, vol. 8, no. 1, pp. 816-820, 1995.

8. K. S. Om, W. H. Lee, S. Y. Jung, and J. H. Chung, "Symmetric Huffman coding - a new modified Huffman coding scheme," *Korean Signal Processing Conference*, vol. 8, no. 1, pp. 847-851, 1995.

9. K. S. Om, D. H. Lee, J. W. Kim, J. H. Kim, H. C. Kim, and B. G. Min, "Flow visualization using texture fields," *'96 KOSOMBE Spring Conference*, vol. 18, no. 1, pp. 69-72, 1996.

10. K. S. Om, W. W. Choi, J. M. Ahn, S. K. Park, Y. H. Jo, J. S. Choi, J. J. Lee, H. C. Kim, and B. G. Min, "Experimental approach for the estimation of cardiac output of left ventricular assist device using multi-dimensional interpolation technique," *'96 KOSOMBE Spring Conference*, vol. 18, no. 1, pp. 232-234, 1996.

11. K. S. Om, W. W. Choi, J. M. Ahn, Y. H. Jo, H. C. Kim, and B. G. Min, "Filter design for noise suppression in IVP signals of a Korean-type total artificial heart," *'96 KOSOMBE Fall Conference*, vol. 18, no. 2, pp.268-272, 1996.

12. K. S. Om, H. C. Kim, and B. G. Min, "Multidimensional linear interpolation is a special form of Tsukamoto's fuzzy reasoning," *Proceedings of KFIS Fall Conference '96*, vol. 6, no. 2, pp. 147-150, 1996.

13. K. S. Om, and H. C. Kim, and B. G. Min, "Relation between multidimensional linear interpolation and regularization networks," *Proceedings of KFIS Spring Conference '97*, vol. 7, no. 1, pp. 128-133, 1997.

14. K. S. Om, J. M. Ahn, J. H. Lee, J. H. Choi, W. E. Kim, H. C. Kim, and B. G. Min, "The supervisory control system in a moving-actuator type total artificial heart: thought and progress," *'97 KOSOMBE Spring Conference*, vol. 19, no. 1, pp. 55-58, 1997.

15. K. S. Om, J. M. Ahn, S. K. Park, Y. H. Jo, W. W. Choi, J. S. Choi, H. C. Kim, and B. G. Min, "Can we estimate the LAP, RAP, PAP, AoP and CO from the interventricular pressure and motor current in a moving-actuator type total artificial heart? Yes, we can," *'97 KOSOMBE Spring Conference*, vol. 19, no. 1, pp. 59-63, 1997.

16. K. S. Om, J. M. Ahn, J. H. Chung, H. C. Kim, and B. G. Min, "Balanced trimming technique for order statistic filtering," *Korean Signal Processing Conference*, vol. 10, no. 1, pp. 911-914, 1997.

17. K. S. Om, J. M. Ahn, S. K. Park, Y. H. Jo, H. C. Kim, and B. G. Min, "Static aortic pressure model for a moving-actuator type total artificial heart," *'97 KOSOMBE Fall Conference*, vol. 19, no. 2, pp. 122-125, 1997. pp. 55-58, 1997.

Domestic Journal

1. 엄경식, 정재호, "관상동맥 영상에서의 혈관 경계 검출," *대한의용생체공학회지*, vol. 16, no. 4, pp.439-446, 1995.

2. K. S. Om and J. H. Chung, "Detection of left ventricular contours based on elliptic approximation and ML estimate in angiographic images," *J. Electrical Engineering and Information Science*, vol. 1, no. 2, pp. 9-14, June, 1996.

3. K. S. Om and B. G. Min, "Relation between multidimensional linear interpolation and fuzzy reasoning," *J. Korea Fuzzy Logic and Intelligent Systems*, vol. 6, no. 4, pp. 34-38, 1996.

4. K. S. Om and B. G. Min, "Relation between multidimensional linear interpolation and regularization networks," *J. Korea Fuzzy Logic and Intelligent Systems*, vol. 7, no. 3, pp. 89-95, 1997.

5. K. S. Om, J. M. Ahn, W. W. Choi, S. K. Park, S. J. Kim, Y. H. Jo , J. S. Choi, J. H. Lee, J. H. Choi, H. C. Him, and B. G. Min, "A study on the practical estimation of nonlinear hemodynamic variables for the moving-actuator type total artificial heart," *J. Korea Society of Medical and Biological Engineering*, vol. 19, no. 2, pp. 153-161, 1998.

6. K. S. Om, H. C. Kim, B. G. Min, C. S. Shin, and H. G. Lee, "Statistical RBF network with applications to an expert system for characterizing diabetes mellitus," *J. Electrical Engineering and Information Science*, vol. 3. no. 3, pp. 355-365, 1998.

7. K. S. Om, J. M. Ahn, Y. H. Jo, Y. N. Park, W. E. Kim, S. H. Cho, W. G. Kim, J. R. Roh, T. H. Won, H. C. Kim, and B. G. Min, “Artificial heart control,” *J. Korea Society of Medical and Biological Engineering*, vol. 20, no. 6, pp. -, 1999.

International Conference

1. K. S. Om W. H. Lee, S. Y. Jung, and J. H. Chung, "Symmetric Huffman coding," *Int. Conf. Electronics, Information, and Communication*, China, pp. 376-379, 1995.

2. K. S. Om, H. C. Kim, and B. G. Min, "Relations among the multidimensional linear interpolation, fuzzy reasoning, and neural networks," *Asian Fuzzy Systems Symp.*, Korea, vol. 3, pp. 562-567, 1998.

3. K. S. Om, J. M. Ahn, Y. H. Jo, W. E. Kim, Y. N. Park, H. C. Kim, W. G. Kim, and B. G. Min, “Fuzzy logic and knowledge based automatic control of the moving-actuator type totally implantable artificial heart,” *IEEE Int. Conf. Fuzzy Systems*, Korea, vol. 8, pp. 149-153, 1999.

4. K. S. Om, J. M. Ahn, C. Y. Park, G. J. Yun, H. S. Cho, J. W. Kim, Y. H. Jo, W. E. Kim, Y. N. Park, J. S. Choi, J. W. Park, S. W. Choi, W. G. Kim, and B. G. Min, “The automatic control of the moving-actuator type totally-implantable artificial heart using the motor current,” *Asia-Pacific Conf. Medical and Biological Engineering*, Korea, vol. 4, pp. 562-567, 1999.

International Journal

1. K. S. Om, J. M. Ahn, and B. G. Min, "Static state hemodynamic variables estimation model for the moving-actuator type total artificial heart. Part. I - cardiac output estimation, " *Int. J. Artificial Organs*, vol. 22, no. 1, pp. 21-26, 1999.

2. K. S. Om, Y. H. Jo, and B. G. Min, "Static state hemodynamic variables estimation model for the moving-actuator type total artificial heart. Part. II - aortic pressure estimation, " *Int. J. Artificial Organs*, vol. 22, no. 2, pp. 108-112 , 1999.